To the Graduate Council:

I am submitting herewith a thesis written by Nicolas Alvertos entitled "Omnidirectional Robot Vision: Correction and Restoration of Fish-eye Lens Images." I have examined the final copy of this thesis for form and content and recommend that it be accepted in partial fulfillment of the requirements for the degree of Master of Science, with a major in Electrical Engineering.

Ernest L. Hall, Major Professor

We have read this thesis
and recommend its acceptance:

Ign Aleksoff

Donald W. Bouldin

Accepted for the Council:

The Graduate School

OMNIDIRECTIONAL ROBOT VISION: CORRECTION AND RESTORATION OF FISH-EYE LENS IMAGES

A Thesis

Presented for the

Master of Science

Degree

The University of Tennessee, Knoxville

Nicolas Alvertos

August 1983

Στούς γονείς μου

ABSTRACT

The purpose of this study was to describe techniques for geometric and blurring restoration of fish-eye lens images. The history of extreme wide angle imaging is briefly reviewed, with most emphasis on previous experiments and theories developed on the fish-eye lens subject. Fish-eye lens images, which can include a 2π steradian field of view, appear with an unavoidable inherent distortion which can be corrected with image processing techniques. A method for geometric restoration of such distorted images is derived, based on a simple pinhole camera model, and its resolution is examined. In a more detailed examination of the model, it is shown that the fish-eye image can be transformed from a space variant system into a space invariant one. An example is given of the application of this transformation to "undistort" a photograph made through a fish-eye lens. After geometric restortion, the image can be further enhanced by applying deblurring techniques to improve resolution. An example is given of the results of deblurring applied to the geometrically restored image from the previous example. Finally, an image correction system that would interact with a computer was suggested for hardware implementation.

TABLE OF CONTENTS

CHAPTER		PAGE
I.	INTRODUCTION	1
II.	PROJECTION METHODS--MAXWELL'S FISH-EYE LENS	10
	Regular Lens Projection [Miyamoto]	10
	Stereographic Projection [Beck and Miyamoto]	12
	Equidistant Projection [Beck and Miyamoto]	12
	Equisolid Angle Projection [Miyamoto]	12
	Orthographic Projection [Beck]	13
III.	GEOMETRIC RESTORATION	21
	Regular Lens Projection	25
	Stereographic Projection	27
	Equidistant Projection	27
	Equisolid Angle Projection	28
	Orthographic Projection	28
IV.	RESOLUTION AND ERROR ANALYSIS	39
V.	DEBLURRING OF THE RESTORED IMAGE	53
	Ideal Highpass Filter	57
	Butterworth Highpass Filter	57
	Trapezoidal Highpass Filter	58
	Exponential Highpass Filter	58
VI.	CORRECTION SYSTEM DESCRIPTION	66
VII.	CONCLUSIONS	75
LIST OF REFERENCES		77
APPENDICES		79
	Appendix A	80
	Appendix B	82
	Appendix C	83
VITA		84

LIST OF FIGURES

FIGURE		PAGE
1.1.	View as seen by a fish	3
1.2.	Typical fish-eye lens construction	5
1.3.	Range of focal length on lenses available from Canon	6
2.1.	The fish-eye lens as a hemispherical model	11
2.2.	Relation between r and θ for different projections	14
2.3.	Relation between r and θ in equisolid angle projection	15
2.4.	Graphical relation between a location γ and the corresponding refractive index $\eta(\gamma)$ in a sphere	17
3.1.	Geometry for a pinhole camera	22
3.2.	Graph of the non-linear relation between the distance in the fish-eye image, r, and the distance in the corrected image, r'	26
3.3.	Geometry of the fish-eye lens model	30
3.4.	Example of correction procedure	37
4.1.	Restoration mappings and transformations	41
4.2.	General approach to complete restoration	45
4.3.	Error curve for the fish-eye lens system	50
5.1.	Example of the deblurring procedure	54
5.2.	Detailed procedure for improving a blurred image	60
5.3.	Illustrations of density functions	64
5.4.	Histograms of images	65
6.1.	Block diagram of correction system	67

FIGURE PAGE

6.2. Four fish-eye images describing a vertical motion sequence 69

6.3. Partially corrected images corresponding to those in Figure 6.2 70

6.4. Four fish-eye images describing a horizontal motion sequence 72

6.5. Partially corrected images corresponding to those in Figure 6.4 73

6.6. A normal 50 mm lens image and a fish-eye lens image . 74

CHAPTER I

INTRODUCTION

Image processing techniques are now being widely used in many important areas, such as space research, medical imaging, and military applications. A vivid demonstration of this modern technology has been provided by the striking images of scenes never before seen by humans recently received from the Viking, Mariner, and Voyager spacecrafts. The image enhancement and distortion correction techniques applied to these images by NASA at the Jet Propulsion Laboratory are now expected by the public. The computed tomography technique for medical imaging, for which the Nobel prize was awarded just a few years ago, is another striking example. This technique, the result of technology less than ten years old, is now available in commercial instruments. X-ray images, for example, are enhanced and processed with the use of those instruments so that a precise diagnosis can be concluded.

In the military area, modern cruise missile technology also uses advanced image processing techniques. Image matching, in which an image of a target is used as a reference and comparison for locating the target in a sensed image, is the basis of high accuracy missile guidance systems. These techniques are more fully described in a recent book on computer image processing [1].

Although striking improvements and developments have been made in image processing techniques and devices, it appears that very little

has been done in the development of omnidirectional optical imaging. Current omnidirectional optical, radar, or other electro-magnetic spectral range sensors require a mechanical scan in order to obtain a full 2π field of view. Although this works quite well in many applications, mechanical scanning devices may fail. More fundamentally, the mechanical scanning is time response limited by the scanning time required to provide the full field of view coverage. In military and security applications, the motion of the scanning device may also be undesirable.

The optical lenses with the widest field of view are often called fish-eye lenses, since the view recorded is similar to that seen by a fish under water, as illustrated in Figure 1.1. Virtually everything within a 2π steradian field of view may be seen by a fish because of the refraction between water and air. Lines near the center of the field of view are distorted very little; however, away from the center, either horizontal or vertical non-radial lines are transformed into curves.

The view as seen by a fish (or human) under water is shown in Figure 1.1. This image formation process is based on Snell's law of refraction, which states that

$$\frac{\sin I}{\sin R} = \frac{\eta_R}{\eta_I} ,$$

where I is the angle between the incident ray and the surface normal at the point the ray enters the different medium, R is the angle between the refracted ray and the surface normal at the point the ray

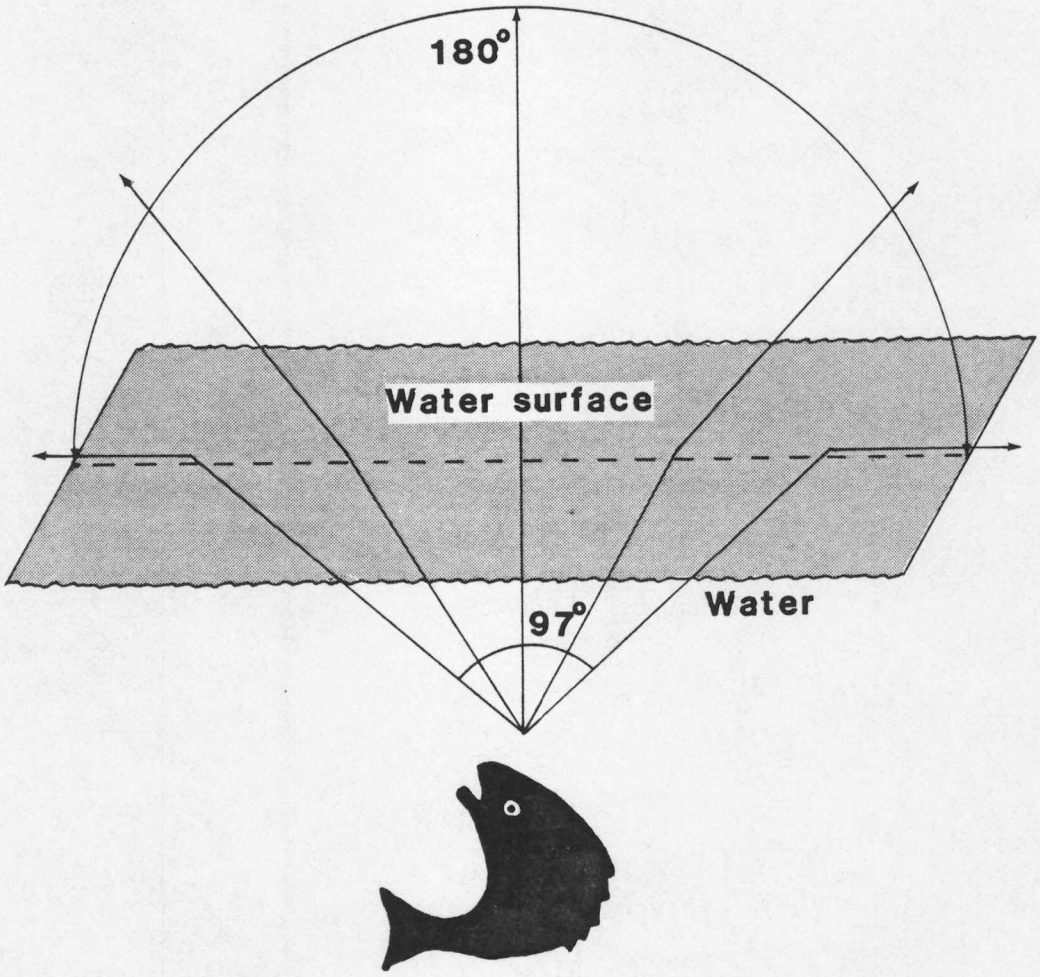


Figure 1.1. View as seen by a fish.

exits the medium, and η_I, η_R are the refractive indices for the two media where I and R are located respectively. For an air and water interface, the ratio η_R/η_I is approximately 1.33. When I = 90°, sin R = 0.75 or R = 48.6°, which is the critical angle of refraction in water.

Franke [2] described a 2π steradian pinhole camera made by placing a hemispherical lens behind a pinhole. This system mapped the 2π steradian view onto the film plane inside a cone of 84°. To achieve the complete coverage of a 2π steradian field of view with a normal 50mm lens would require about 25 separate exposures with substantial overlap.

A modern optical fish-eye lens is a complex design in which the front element is a miniscus with a deeply concave rear surface. A typical fish-eye lens construction is shown in Figure 1.2. This miniscus front lens refracts the light rays from a 2π steradian field of view into a cone of approximately 90°. A secondary lens system is used to provide various corrections such as chromatic aberration, etc., and focuses the image on the recording medium or detector. There is usually no focusing mechanism provided for a fish-eye lens, as it inherently has a large depth of field.

The principal difference between fish-eye lenses and super wide-angle lenses is that the super wide-angle lenses are optically corrected to render straight lines as straight lines. The relationship between the fish-eye and other lenses available from the Canon Co. is shown in Figure 1.3. Note that the widest field of view offered is 104° [3]. This limit indicates the amount of distortion

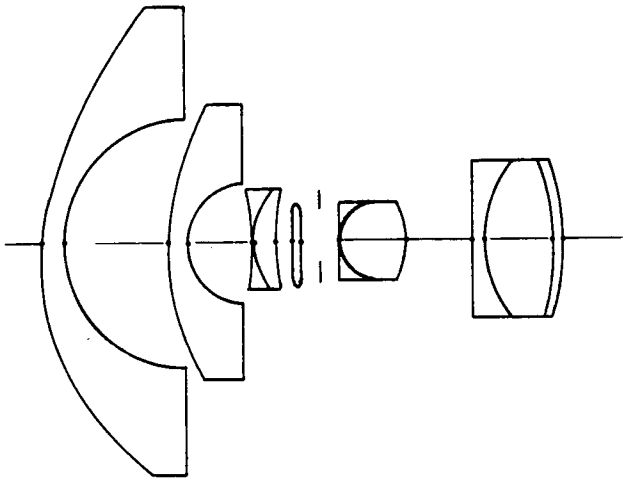


Figure 1.2. Typical fish-eye lens construction.

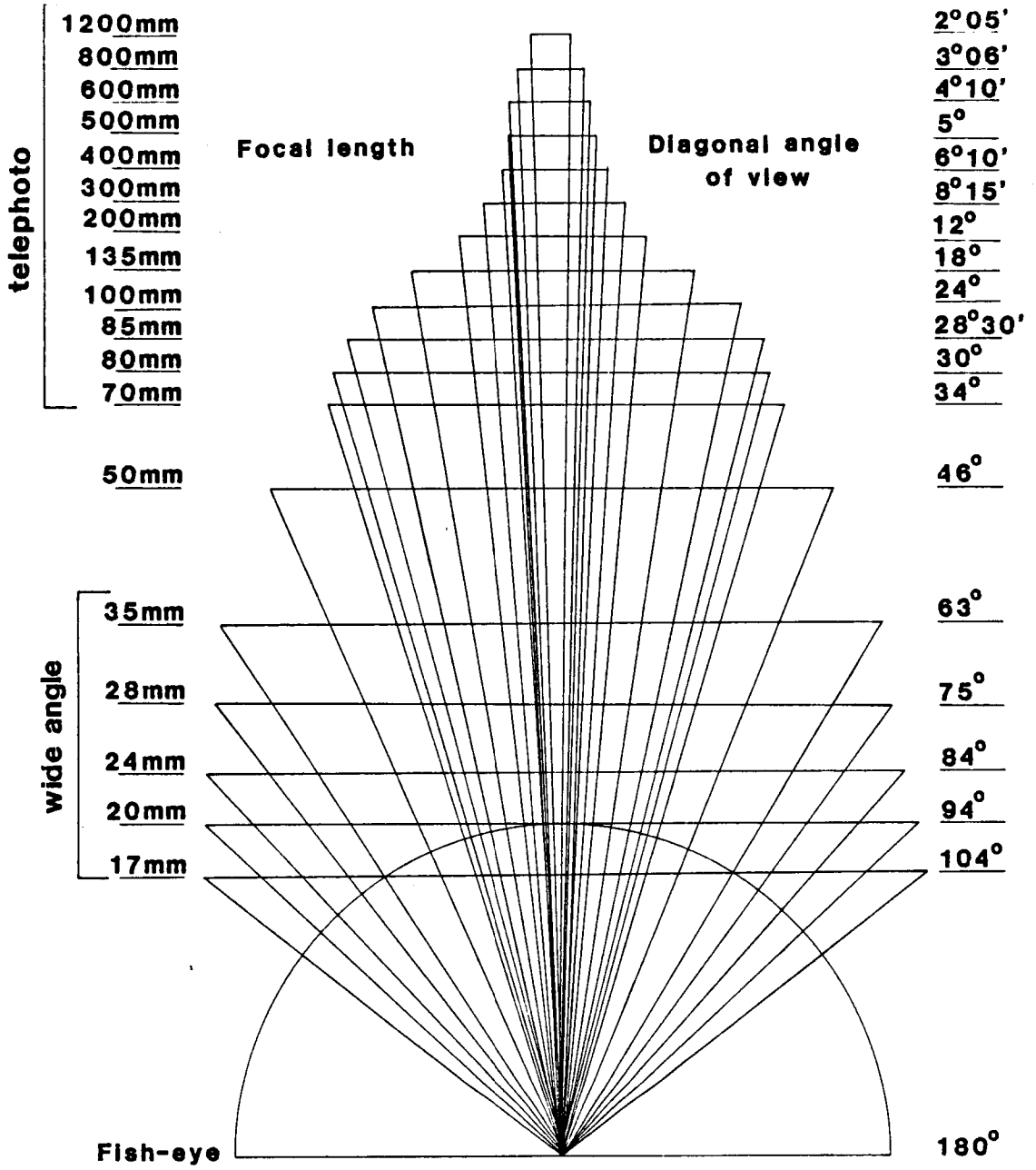


Figure 1.3. Range of focal length on lenses available from Canon.

that can be corrected by optical design alone. Current studies in wide-angle and "fish-eye" lens design were considered at a recent lens design conference [4,5].

A classical example of the fish-eye lens was given by Wood [6], who took a 2π steradian photograph with a pinhole camera filled with water. Bond [6] substituted a hemispherical lens with a pupil at the center of curvature for the water in the pinhole camera. Hill [6] developed a lens combination consisting of a large front lens with a curved convex outer surface and a very deep concave inner surface. A compound photographic lens was placed behind the front lens, as well as a holder for apertures and color filters. The astigmatism and curvature of field were corrected by the combination of the three lenses. Chromatic errors, especially at the edges of the field, were reduced by making multiple exposures with color filters.

A method for correcting the distortion inherent in the fish-eye lens was described by Beck [7]. He realized that with a fish-eye image, it was possible to produce a number of normal photographs such as would be seen by a camera pointing in the desired direction by reversing the recording action and projecting a negative of the fish-eye image back through the lens. He produced images which clearly show the curvature recorded in the fish-eye image projected back into straight lines.

The inherent distortion of the fish-eye lens is induced when a 2π steradian hemisphere is projected onto a plane circle. Cartographers have devised many ways to map these projections. Each method leads to a particular distortion and requires a unique correction.

Among other problems, however, the fundamental problems of refraction and refractive index arise, since the fish-eye lens is modeled as a hemispherical lens, as will be seen later. The term "fish-eye lens" was first introduced by Maxwell in 1854 when he developed "the law of the index of refraction in a spherical medium" and noted that a medium with such optical properties may exist in the structure of the crystalline lens in fish [8]. The particular properties of the fish-eye were demonstrated in a paper by Demkov and Ostrovskii [9], where a stereographic projection of the three-dimensional space was performed onto a four-dimensional sphere.

Although a stereographic projection will demonstrate the properties of the spherical fish-eye medium, it will be shown that the hemispherical fish-eye system results in and is considered as an equisolid angle projection. In examining the resolution and restoration of such a projection, the point spread function of the system must be determined. The point spread function of an optical system may be either space variant, that is, varies with the object and image position, or space invariant, that is, depends only on the difference in location [10]. It may be shown that the fish-eye lens system is a space variant one, and that its point spread function may be determined by evaluating the Jacobian. The study, therefore, of the geometric correction and restoration of the system is completed.

Such a process, however, would produce a considerable amount of blurring to the final restored image. In addition, depending on the resolution (pixel size) of the digital image, blurring due to magnification is apparent. In an article by Fahnestock and Hunt [11],

the maintenance of sharpness in a magnified digital image is discussed, and approaches for such an accomplishment are described. A suggested approach is that of designing a filter which would affect only the high-frequency information of the image. Several high-frequency filters and general filtering techniques for "sharpening" an image and, thus, improving its quality are discussed by Gonzalez and Wintz [12].

A complete correction system has been proposed in a recent article by Anderson, Alvertos, and Hall [13], where an arrangement using two fish-eye lenses would provide a full 4π steradian coverage. In addition, in the same article [13], a comparison of the human eye mechanism and the proposed one is described, along with the use of a computer as a control interface to the correction system.

CHAPTER II

PROJECTION METHODS--MAXWELL'S FISH-EYE LENS

As an illustration of the projection of the 2π steradian hemisphere onto a plane circle, mentioned in the previous chapter, several methods to accomplish such a mapping are presented in this chapter.

Consider the simplified model shown in Figure 2.1. If θ is the angle between the incident ray and the optical axis and ϕ is the corresponding angle between the refracted ray and the optical axis, then the distortion may be described by relating θ and ϕ. If the fish-eye is modeled as a pinhole camera with the image plane located a distance D behind the center, then a point at distance r from the center of the image is described by $r = D \tan \phi$.

Several mappings can now be described by relating θ and ϕ. Beck [7] and Miyamoto [6] described several types with advantages and disadvantages.

Regular Lens Projection [Miyamoto]

For this type of projection, $\phi = \theta$ and, therefore, $\tan \phi = \tan \theta$. Thus, the image r may be described in terms of θ and, since $r = D \tan \phi$, we have that $r = D \tan \theta$.

With this regular lens projection, a small circle facing the camera will map into a circle on the image.

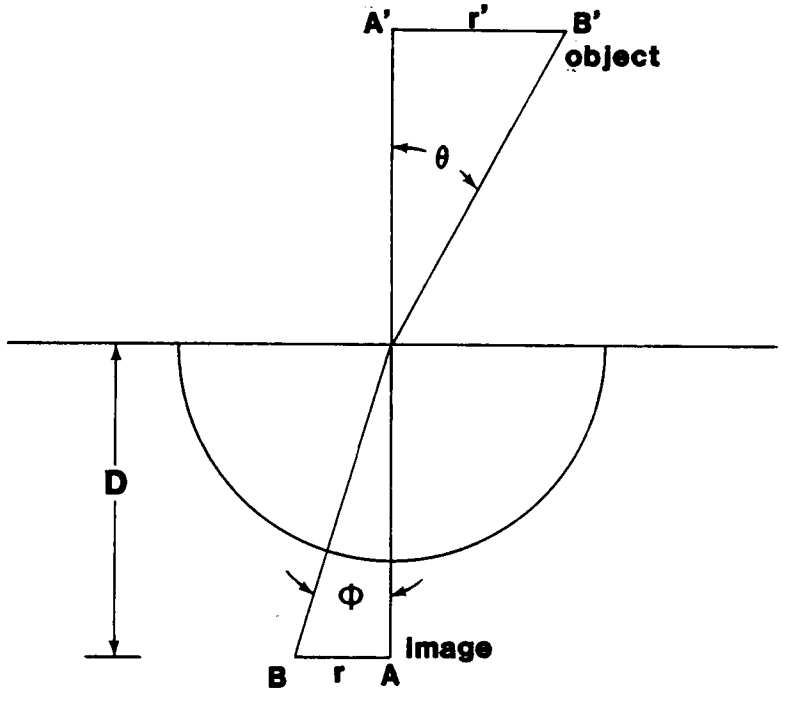


Figure 2.1. The fish-eye lens as a hemispherical model.

Stereographic Projection [Beck and Miyamoto]

In stereographic projection, θ and ϕ are related as follows: $\tan \phi = 2 \tan (\theta/2)$ and, for this case, r can be expressed in terms of θ and be: $r = 2 D \tan (\theta/2)$.

Beck noted that with this propjection, a small circle facing the camera will always map into a small circle on the image plane, but the diameter of the image of the circle will increase as the circle is moved from the pole to the horizon. Miyamoto also noted that this projection is similar to the human perception of the sky.

Equidistant Projection [Beck and Miyamoto]

In such a projection, θ and ϕ are related as follows: $\tan \phi = \theta$ and, thus, $r = D\theta$.

Beck notes that the result of such a projection of a circle would be an ellipse-like figure toward the image edge with one diameter always remaining the same. Miyamoto noted that this projection was preferable for measurement of zenith and azimuth angles since the effect of lens position error is small, and the linear relation between r and θ is convenient to analyze.

Equisolid Angle Projection [Miyamoto]

In an equisolid angle projection, $\tan \phi = 2 \sin (\theta/2)$ and, thus, r can be expressed as $r = 2 D \sin (\theta/2)$.

Miyamoto referred to this as equisolid angle projection because the solid angle Ω is proportional to the corresponding area A on the image plane.

The above statement may be shown as follows: Since $r = 2D \sin(\theta/2)$, then $dr = D \cos(\theta/2)\, d\theta$. Therefore, $rdr = D^2\, 2 \sin(\theta/2) \cos(\theta/2)\, d\theta$. However, $\sin\theta = 2 \sin(\theta/2) \cos(\theta/2)$ and, thus, $rdr = D^2 \sin\theta\, d\theta$. Multiplying the last relation by $d\phi$, we obtain: $rdr\, d\phi = D^2 \sin\theta\, d\theta\, d\phi$, and, since $d\Omega = \sin\theta\, d\theta\, d\phi$ and $dA = rdr\, d\phi$, we have $dA = D^2 d\Omega$ or $d\Omega = dA/D^2$, which suggests that the solid angle Ω is proportional to the corresponding area A on the image plane.

Miyamoto noted that this mapping could be used for measuring the percentage of sky covered by clouds or obstructed by buildings.

Orthographic Projection [Beck]

The relation between θ and ϕ, in orthographic projection, is given by $\tan\phi = \sin\theta$. An expression, then, for r can be obtained in terms of θ and it is $r = D \sin\theta$.

Beck noted that this was a less satisfactory mapping in which the circle is mapped so that one diameter increases and the other decreases until the edge of the circle is represented by a line.

Relations between r and θ are shown in Figures 2.2 and 2.3 for all the projections described above.

Each of the above projections is considered as the result of projection of a hemisphere on a plane which produces the distortion of the fish-eye lens. The distortion should not be considered as an aberration in which case color filters must be employed for the necessary correction [6]. As will be shown in the next chapter, the projection resulting from the fish-eye lens model could be any of the above projections. Figure 2.3 shows the relation between the image r

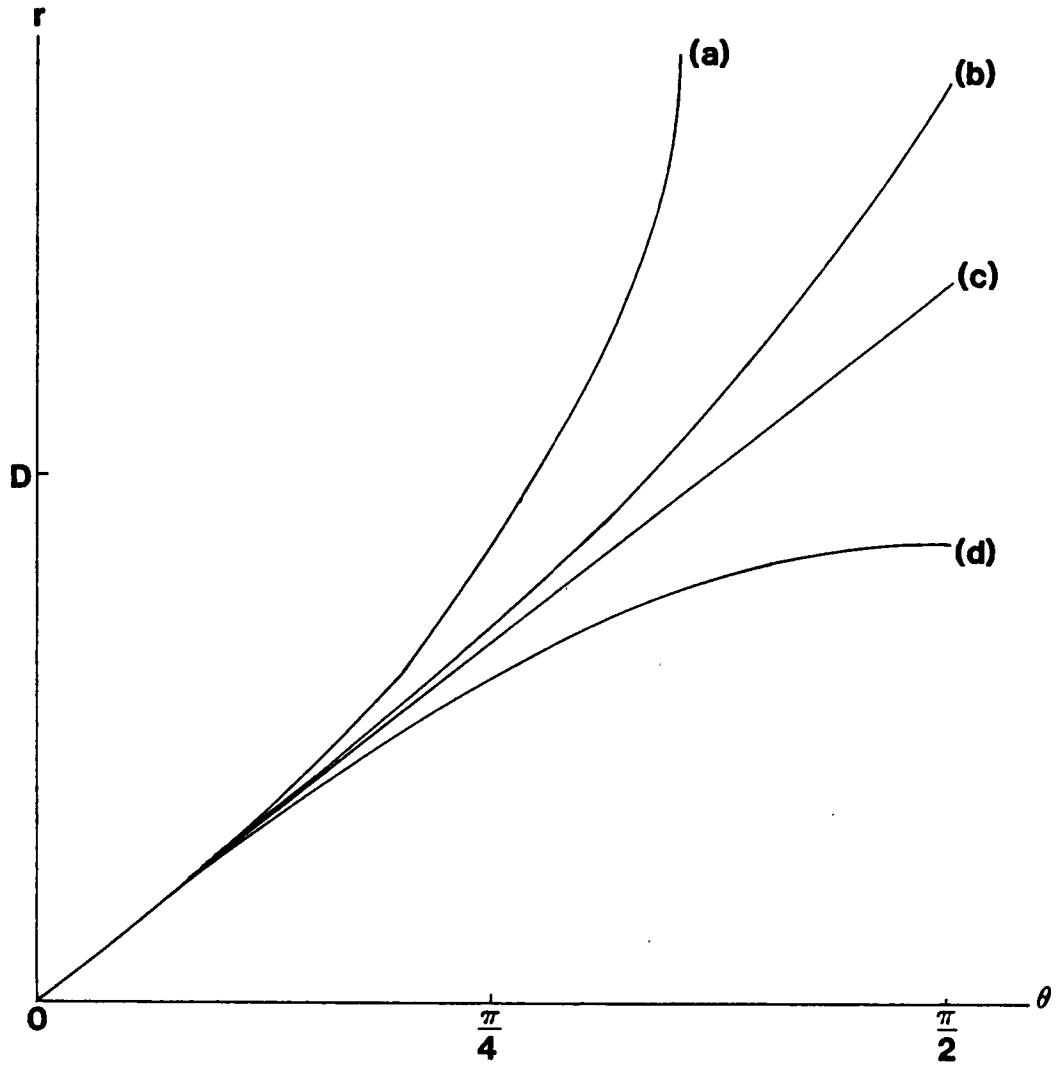


Figure 2.2. Relation between r and θ for different projections.

(a) Regular lens projection.
(b) Stereographic projection.
(c) Equidistant projection.
(d) Orthographic projection.

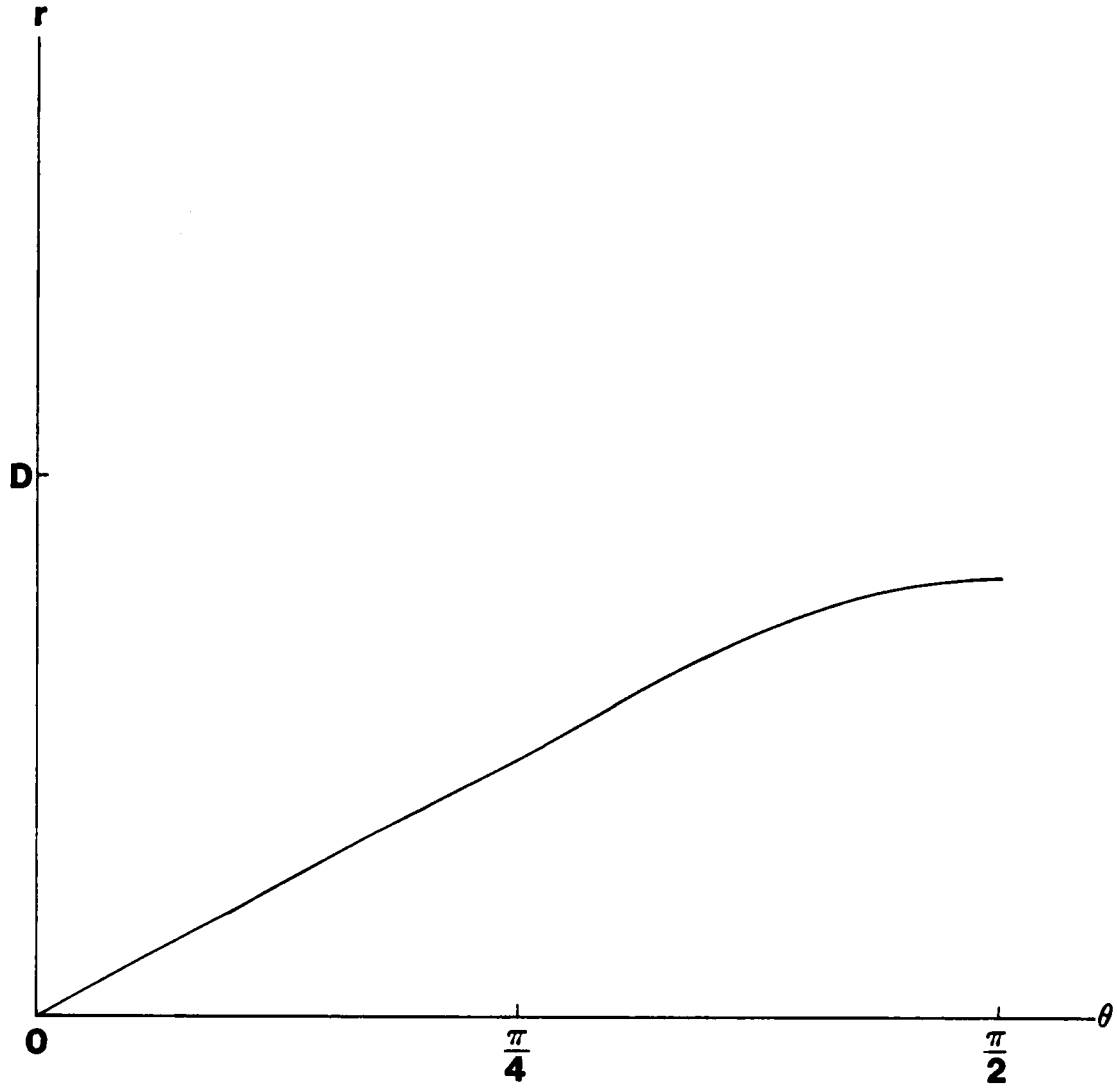


Figure 2.3. Relation between r and θ in equisolid angle projection.

and the incident angle θ of the model in Figure 2.1. The shape of the curve is similar to that relating the image and the incident angle in equisolid angle projection.

Although aberration should not be considered within the inherent distortion of the fish-eye lens, as it was mentioned above, it exists wherever a spherical medium is involved. It should, therefore, be considered for the hemispherical model employed here. Maxwell, in 1854 [8], found that the refractive index η of a sphere of radius ρ is a function of the location the refractive index is referring and is given by

$$\eta(\gamma) = \frac{2\eta'}{1 + (\gamma/\rho)^2} \qquad (2.1)$$

where $\eta(\gamma) = \eta'$ when $\gamma > \rho$. The relation between $\eta(\gamma)$ and the location γ, for (2.1), is illustrated in Figure 2.4. Maxwell, by obtaining relation (2.1), established the focusing properties of the spherical system which he called the fish-eye problem [9]. He supported that all rays in a spherically symmetric optical system were circles, from the fact that the stereographic image of an arbitrary circle on the sphere is a circle [9].

Let the surface of the sphere with radius ρ, in relation (2.1), be S. It has been shown that all rays leaving a point on the surface of the sphere, S, in the inward direction are focused at the point diametrically opposite on S [9]. In such a case, all the rays are either circles or straight lines intersecting S at diametrically opposite points. In addition, the refractive index given by relation

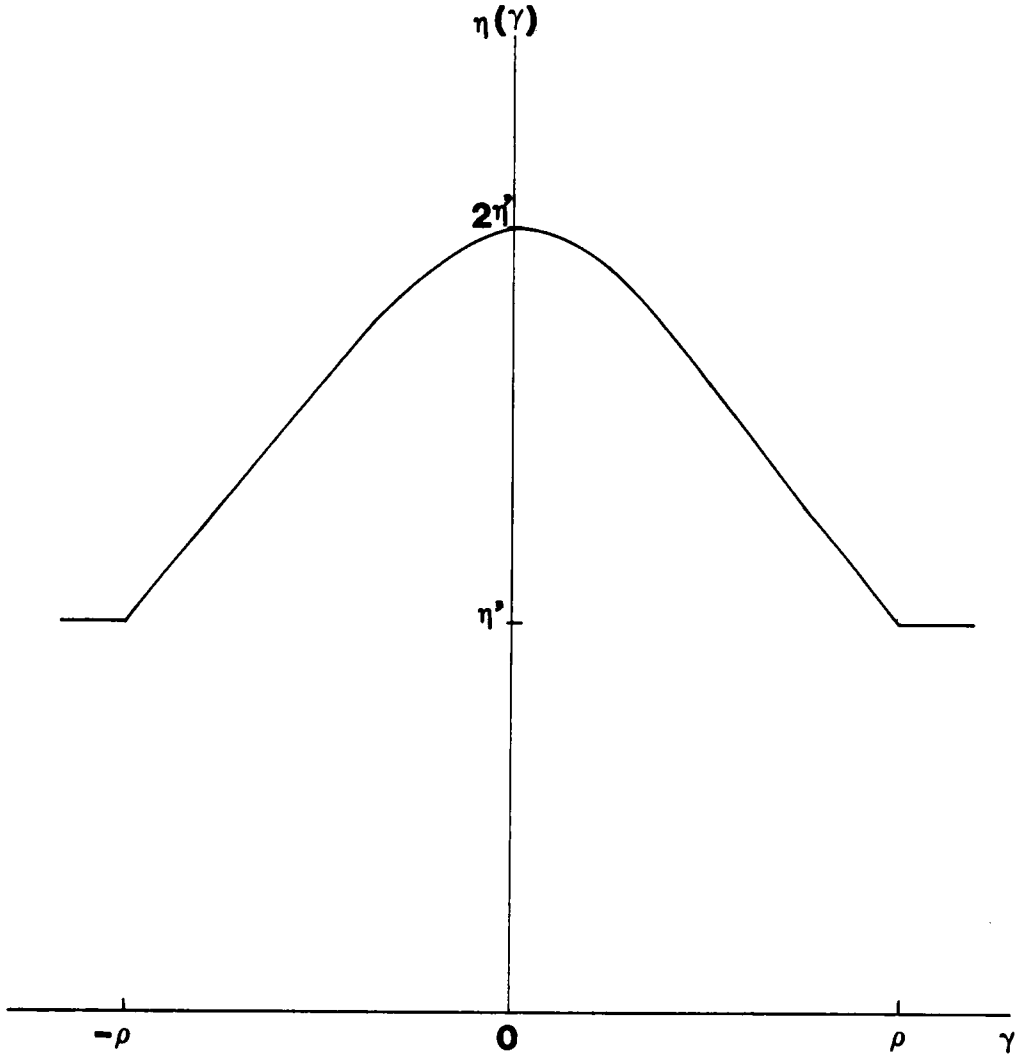


Figure 2.4. Graphical relation between a location γ and the corresponding refractive index $\eta(\gamma)$ in a sphere.

(2.1) will exactly focus rays leaving any point in space and not only points from S; in fact, all rays leaving a point located at γ are found to pass through the point located at $\gamma\rho^2/\gamma^2$ [9].

To demonstrate the particular properties of the fish-eye, Demkov and Ostrovskii [9] performed a stereographic projection of the three-dimensional space onto a four-dimensional sphere of surface S and radius ρ. Assuming that the point $(\zeta_1,\zeta_2,\zeta_3,\zeta_4)$ lies in a unit sphere in the four-dimensional space, then, a point (χ,ψ,ω) is projected onto the point $(\rho\zeta_1,\rho\zeta_2,\rho\zeta_3,\rho\zeta_4)$. The coordinates of the four-dimensional space are described in terms of χ,ψ,ω, the radius of the sphere ρ and the arbitrary position γ:

$$\zeta_1 = \frac{2\rho\chi}{\rho^2 + \gamma^2}, \qquad \zeta_2 = \frac{2\rho\psi}{\rho^2 + \gamma^2},$$
$$\zeta_3 = \frac{2\rho\omega}{\rho^2 + \gamma^2}, \qquad \zeta_4 = \frac{\rho^2 - \gamma^2}{\rho^2 + \gamma^2}. \tag{2.2}$$

Since in stereographic projection a circle will map onto a circle [7], the rays through the spherical medium transform into the major circles of the four-dimensional sphere. Circles that pass through a point on S will intersect at a diametrically opposite point, on S, as mentioned above. This fact explains the focusing properties of the fish-eye (spherical) medium [9].

Demkov and Ostrovskii [9] also noted that Maxwell's fish-eye problem is related to the Coulomb problem. Assuming, for example, that an electron with energy E moves on an ellipse in the Coulomb potential $V_c = - Q/\gamma$, the orbits in momentum space [9] are identical

with the paths of the motion of a particle with mass equal to unity and zero energy in a potential

$$V_j(\gamma) = - \frac{2\tau}{(\rho^2 + \gamma^2)^2} , \tag{2.3}$$

where τ is an arbitrary parameter and $\tau > 0$, if

$$\rho^2 = - 2E. \tag{2.4}$$

For a potential, $V(\gamma)$, which is monotonic and spherically symmetric, the "action function in momentum space" [9] is

$$H(\bar{p},\bar{p}',E) = \int_{p'}^{p} \bar{\gamma} d\bar{p}, \tag{2.5}$$

where the points p and p' are joined by the particle's motion path and the integral is evaluated in momentum space [9]. Relation (2.5) satisfies the differential equation

$$(\frac{\partial H}{\partial p_\chi})^2 + (\frac{\partial H}{\partial p_\psi})^2 + (\frac{\partial H}{\partial p_\omega})^2 - [\gamma(E - \frac{p^2}{2})]^2 = 0, \tag{2.6}$$

where γ is meant as $\gamma(V)$ which is the inverse of $V(\gamma)$ [9]. If $Q^2 = \tau$ and simultaneously relation (2.4) is satisfied, then, for the Coulomb potential

$$\gamma(V) = \frac{2Q}{V^2 - 2E} , \tag{2.7}$$

relation (2.6) becomes identical with the Hamilton-Jacobi equation for the Maxwell problem by replacing the momenta by the coordinates [9], which describes a symmetrical optical system with the focusing properties mentioned above.

Symmetry and exact focusing, which explains the fact that no focus adjustment is needed for the fish-eye, are not the only properties of the system. Maxwell [8] also found that the law of the index of refraction will give a minimum of aberration for a sphere with variable refractive index, such as described in relation (2.1), placed in water.

Theoretically, therefore, it is possible to construct spherically symmetric systems which have ideal focusing properties and are perfect for homogeneous light. However, the proposed hemispherical model in this study will be assumed to be of a medium with a constant refractive index. Furthermore, correction of chromatic aberration will not be considered since only black and white images are examined.

CHAPTER III

GEOMETRIC RESTORATION

The geometrical correction required to map the image formed by a fish-eye lens onto a corrected image will be derived in this chapter. The basic geometry of a 2π steradian lens model is shown in Figure 2.1, page 11, which is a cross-section view of a pinhole imaging system with a hemispherical concentrator such as that described by Franke [2].

Assume that an image has been acquired as shown in Figure 3.1. From an image point B at a distance x_0 from the axis of the lens located on the image plane at a distance y_0 from the pinhole aperture, it is desired to derive a corrected location B'(x',y') for this point in the plane of the projected image at an arbitrary distance R from the lens as shown in Figure 3.1. Assuming that D, depending on the object position, is the distance from the center of the lens to the image, then the corrected location r' (object position) of an image r is derived. Referring to Figure 3.1, since the incident ray from r' creates an angle θ with the vertical axis of the lens and the refracted ray to r creates an angle ϕ with the vertical axis, the following relations are obtained:

$$r' = R \cdot \tan \theta \tag{3.1}$$

and

$$r = D \cdot \tan \phi. \tag{3.2}$$

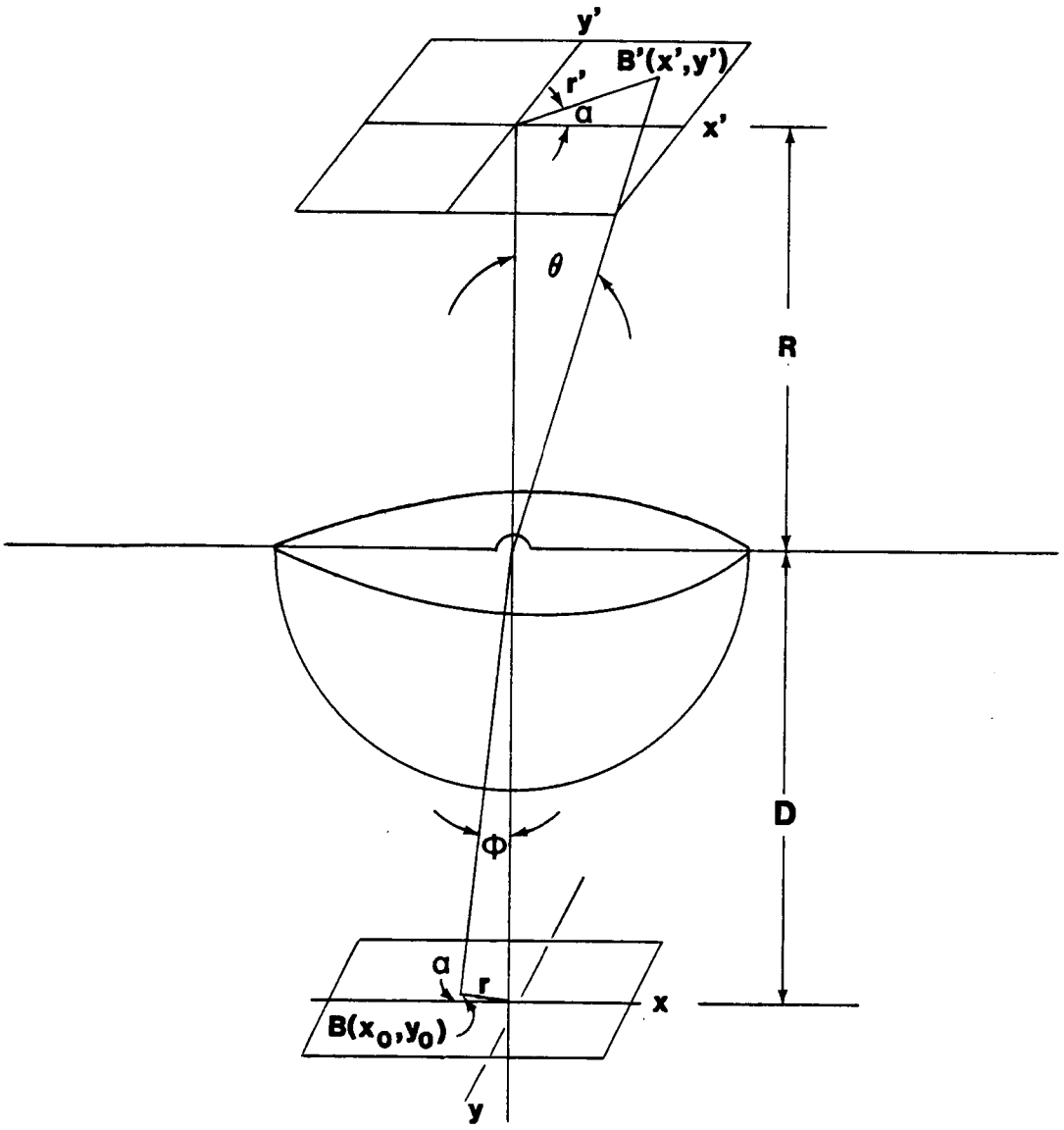


Figure 3.1. Geometry for a pinhole camera.

Dividing relation (3.1) by (3.2) and solving for r', we have:

$$r' = r \frac{R}{D} \frac{\tan \theta}{\tan \phi} = r \frac{R}{D} \frac{\sin \theta}{\sin \phi} \frac{\cos \phi}{\cos \theta} . \tag{3.3}$$

From Snell's law of refraction, the sines of angles ϕ and θ are related as follows:

$$\frac{\sin \phi}{\sin \theta} = \frac{\eta_\theta}{\eta_\phi} = \eta, \tag{3.4}$$

where η_ϕ is the refractive index of the hemispherical medium and η_θ is the refractive index of the medium outside the hemisphere. Calling η (the relative index of refraction) the ratio between η_θ and η_ϕ and substituting relation (3.4) into (3.3), we obtain:

$$r' = r \frac{R}{D} \frac{1}{\eta} \frac{\cos \phi}{\cos \theta} = r \frac{R}{D} \frac{1}{\eta} \frac{\sqrt{1 - \sin^2 \phi}}{\sqrt{1 - \sin^2 \theta}} . \tag{3.5}$$

Dividing both numerator and denominator of the right-hand side of (3.5) by sin ϕ and substituting (3.4), we have:

$$r' = r \frac{R}{D} \frac{1}{\eta} \frac{\sqrt{\csc^2 \phi - 1}}{\sqrt{\csc^2 \phi - \frac{1}{\eta^2}}} = r \frac{R}{D} \frac{\cot \phi}{\sqrt{\eta^2 \cot^2 \phi + \eta^2 - 1}} . \tag{3.6}$$

Since from relation (3.2) we have that $\tan \phi = \frac{r}{D}$, then $\cot \phi = \frac{D}{r}$ which is substituted in relation (3.6) to obtain:

$$r' = r \frac{R}{D} \frac{\frac{D}{r}}{\sqrt{\eta^2 \frac{D^2}{r^2} + \eta^2 - 1}} . \qquad (3.7)$$

Multiplying both numerator and denominator of the right-hand side of (3.7) by r and simplifying, r' is given by:

$$r' = \frac{Rr}{\sqrt{\eta^2 D^2 + (\eta^2 - 1)r^2}} . \qquad (3.8)$$

That is, r' is given in terms of r with η constant for each specified lens assuming that the media involved are known. Note than when r = 0, then r' = 0. In other words, points on the central axis map onto the center of the image. Object points that belong on the central axis of the lens will not be distorted, as expected, and will be projected as in a regular lens projection.

Using the same mathematical procedure for arriving in relation (3.8) or solving from (3.8) for r, a relation giving r in terms of r' may be obtained:

$$r = \frac{D\eta\, r'}{\sqrt{R^2 + (1 - \eta^2)(r')^2}} , \qquad (3.9)$$

where η is the relative refractive index of the lens as specified above. It is important to note that as r' approaches ∞, in relation (3.9), then r approaches $\frac{D\eta}{\sqrt{1 - \eta^2}}$. That is, r is independent of R and only depends on D and η which are both definite and limited

quantities. Therefore, $\frac{D\eta}{\sqrt{1-\eta^2}}$ is a definite, limited, real quantity when $\eta < 1$. When the medium outside the hemisphere has a refractive index smaller than that of the hemispherical medium, then $\eta < 1$. When $\eta = 1$, then the two media are the same (same refractive index) and, therefore, no refraction exists. The fact that when r' approaches ∞ then r has a limited real value is related to the critical angle of the optical system. Recalling relation (3.4), if the incident angle θ is equal to $\pi/2$, in which case a 180° field of view is covered, then $\phi = \sin^{-1}\eta$ is the critical angle of the system. The relation between r and r' as given in (3.9) is illustrated in Figure 3.2. The shape of the curve suggests that the projection appears to be an equisolid angle projection. The shape of the curve in Figure 2.2, page 14, should be similar to that of Figure 3.2, since the first one illustrates a relation between r and θ and the second one between r and r', where r', from relation (3.1), is a function of θ.

However, before any conclusions are stated, it is necessary to examine the limiting conditions, that is, when the incident angle θ is equal to $\frac{\pi}{2}$, for each of the projections mentioned in Chapter II. For each case, the refractive index of the hemispherical medium will be evaluated and, thus, since the refractive index is assumed to be constant, the material of the lens may be concluded for an ideal projection.

Regular Lens Projection

Recalling from Chapter II, the image r and the incident angle θ are related as follows: $r = D \tan \theta$. As θ approaches $\frac{\pi}{2}$, r

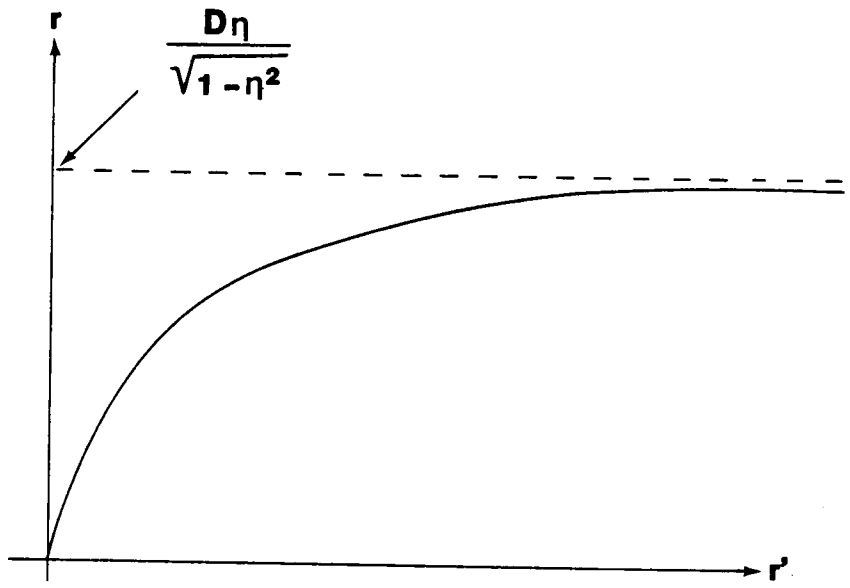


Figure 3.2. Graph of the non-linear relation between the distance in the fish-eye image, r, and the distance in the corrected image, r'.

approaches ∞. Also, recalling relation (3.1), $r' = R \tan \theta$; and as θ approaches $\frac{\pi}{2}$, r' approaches ∞. However, as it has been shown earlier, when r' approaches ∞, then r approaches $\frac{D\eta}{\sqrt{1 - \eta^2}}$, which is a defined quantity. This last result contradicts that previously found where r approaches ∞. Therefore, the fish-eye system cannot result in a regular lens projection.

Stereographic Projection

In stereographic projection, $r = 2D \tan (\theta/2)$. As θ approaches $\frac{\pi}{2}$, r approaches $2D$. Also, since r' approaches ∞ when θ approaches $\frac{\pi}{2}$, r approaches $\frac{D\eta}{\sqrt{1 - \eta^2}}$. Equating the two limits found for r and solving for η (the relative refractive index), it is found that $\eta = 0.89$. Assuming that the medium outside the hemisphere is air ($\eta_\theta = 1$), then, from relation (3.4), the refractive index of the hemispherical medium is $\eta_\phi = 1.12$. Therefore, a fish-eye lens system made of a material with refractive index equal to 1.12 results in a stereographic projection.

Equidistant Projection

Again recalling from Chapter II, the image r and the incident angle θ are related as follows: $r = D\theta$. As θ approaches $\frac{\pi}{2}$, r approaches $\frac{\pi}{2} D$. Also, as has been shown above, for the same conditions, r approaches $\frac{D\eta}{\sqrt{1 - \eta^2}}$. That is, $\frac{D\eta}{\sqrt{1 - \eta^2}} = \frac{\pi}{2} D$ or, solving for η, $\eta = 0.84$. Assuming again that $\eta_\theta = 1$ (air), it is found from relation (3.4) that $\eta_\phi = 1.19$. Thus, a hemispherical lens with refractive index equal to 1.19 results in a stereographic projection.

Equisolid Angle Projection

In equisolid angle projection, $r = 2D \sin(\theta/2)$. As θ approaches $\frac{\pi}{2}$, r approaches $\sqrt{2}\,D$. Also, since r' approaches ∞ when θ approaches $\frac{\pi}{2}$, r approaches $\frac{D\eta}{\sqrt{1 - \eta^2}}$. Equating the two limits of r and solving for η, it gives $\eta = 0.816$. Once more, assuming $\eta_\theta = 1$, solving from relation (3.4) it is obtained $\eta_\phi = 1.225$. Therefore, a fish-eye lens with refractive index equal to 1.225 results in an equisolid angle projection.

Orthographic Projection

The image r and the incident angle θ are related in orthographic projection as follows: $r = D \sin\theta$. As θ approaches $\frac{\pi}{2}$, r approaches D. Also, as has been mentioned above, under the same conditions, r approaches $\frac{D\eta}{\sqrt{1 - \eta^2}}$. Therefore, $\frac{D\eta}{\sqrt{1 - \eta^2}} = D$ or, solving for η, $\eta = 0.707$. Then $\eta_\phi = 1.414$ assuming that the medium outside the hemisphere is air. Thus, a hemispherical lens with refractive index equal to 1.414 results in an orthographic projection.

From the discussion and the previously obtained different values for the refractive index of the fish-eye lens, one could arrive at no definite conclusion as to the type of the projection for this system unless η is known, since the image formation (projection) depends on η, as given in relation (3.9), and a graphic representation of the projection is obtained. Therefore, it is not certain that Figure 3.2 illustrates an equisolid angle projection, since an orthographic projection, shown in Figure 2.2, page 14, is described by a similar type of curve. In addition, the curve of Figure 3.2 has been

obtained by using $\eta = 0.66$; that is, $\eta_\theta = 1$ (air) and $\eta_\phi = 1.5$ (typical refractive index of glass). Thus, the projection for a fish-eye lens made of glass is neither an equisolid angle projection nor an orthographic one.

Although relations (3.8) and (3.9) describe exactly the object and the image, respectively, they are both functions of the distance, D, from the center of the lens to the image r. D, however, is not generally known and rather difficult to acquire. It would be, therefore, useful to obtain a relation between D and some known features of the lens, such as radius and focal length, which are generally known for each lens.

Consider the hemispherical lens with radius ρ shown in Figure 3.3. Let points M' and N' project to points M and N, respectively, and thus an object $r' = \overline{M'N'}$ be creating an image $r = \overline{MN}$, where both N' and N lie on the central axis of the lens that passes through the center, K, of the hemisphere. A ray leaving M' parallel to the central axis will pass through the flat surface of the hemisphere with no refraction, since it is perpendicular to the surface, and continue parallel to the central axis until it intersects with the curved surface of the hemisphere at a point P where it is refracted. The radius $\overline{KP}$ is perpendicular to the curved surface at P creating with $\overline{M'P}$ the incident angle ϕ'. Due to refraction, the extension of $\overline{KP}$ and the refracted ray create the refraction angle θ'. The refracted ray now continues until it intersects the central axis at the focal point Y and, finally, projects to point M. Let $\overline{KY} = f$ be the focal length of the lens measured from the center of the hemisphere and

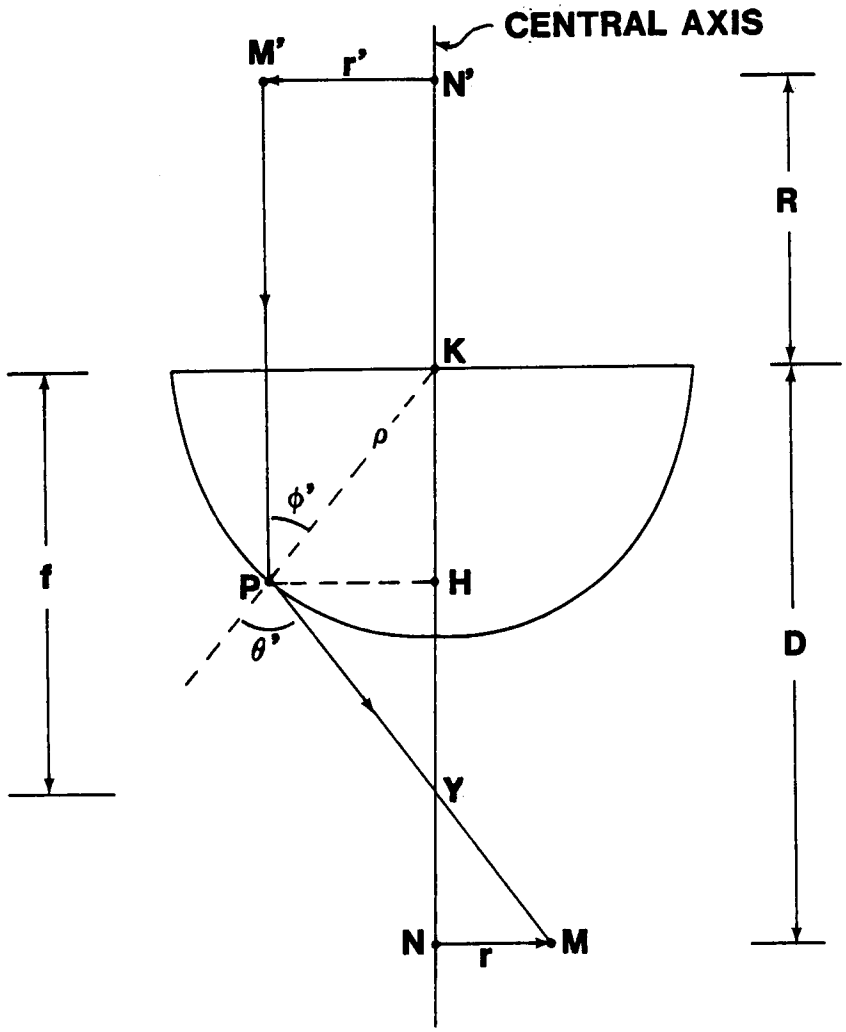


Figure 3.3. Geometry of the fish-eye lens model.

$\overline{KN}$ = D the distance of the image from the center K, as in Figures 2.1, page 11, and 3.1, page 22. Let the perpendicular from P to $\overline{KY}$ be drawn intersecting the central axis at H. Then, triangle YHP is similar to triangle YNM; therefore, since $\overline{PH}$ = r',

$$\frac{r}{r'} = \frac{\overline{YN}}{\overline{YH}} \text{ or, } \frac{r}{r'} = \frac{D - f}{\overline{YH}} \text{ or, solving for D,}$$

$$D = \frac{r}{r'}(\overline{YH}) + f. \tag{3.10}$$

However, $\overline{YH} = f - \overline{KH}$ or, since $\overline{KH} = \sqrt{\rho^2 - (r')^2}$,

$$\overline{YH} = f - \sqrt{\rho^2 - (r')^2}\ . \tag{3.11}$$

Substituting relation (3.11) into (3.10), D is given in terms of the focal length f, the radius ρ, the image r, and the object r':

$$D = \frac{r}{r'}\left[f - \sqrt{\rho^2 - (r')^2}\right] + f. \tag{3.12}$$

To obtain a relation between r and r' involving known quantities, such as f and ρ, (3.12) is substituted into (3.9) that gives r in terms of r', and relation (3.9) becomes:

$$r = \frac{\eta r\left[f - \sqrt{\rho^2 - (r')^2}\right] + f\eta r'}{\sqrt{R^2 + (1 - \eta^2)(r')^2}} \text{ or, solving for r,}$$

$$r = \frac{f\eta r'}{\sqrt{R^2 + (1 - \eta^2)(r')^2} - \eta\left[f - \sqrt{\rho^2 - (r')^2}\right]}\ . \tag{3.13}$$

That is, r is a function of r' with η, f, and ρ constants.

As mentioned earlier, the relative refractive index η depends on the material of the lens, and the focal length f and the radius ρ are generally known. However, if not both f and ρ are known, an approximate relation between these two quantities may be derived. Consider the triangle YPK in Figure 3.3. From the law of sines, since angle PKY = ϕ', angle PYK = $(\theta' - \phi')$ and angle YPK = $(180° - \theta')$, the focal length $f = \overline{KY}$ and the radius ρ are related as follows:

$$\frac{\sin (180° - \theta')}{f} = \frac{\sin (\theta' - \phi')}{\rho} \text{ or, solving for f,}$$

$$f = \frac{\rho \sin \theta'}{\sin \theta' \cos \phi' - \sin \phi' \cos \theta'}, \tag{3.14}$$

since $\sin (180° - \theta') = \sin \theta'$ and $\sin (\theta' - \phi') = \sin \theta' \cos \phi' - \sin \phi' \cos \theta'$. Assuming the same media with refractive indices η_θ and η_ϕ for the hemispherical medium and outside the hemisphere, respectively, then, from Snell's law, angles ϕ' and θ' are related as follows:

$$\frac{\sin \phi'}{\sin \theta'} = \frac{\eta_\theta}{\eta_\phi} = \eta. \tag{3.15}$$

Dividing both the numerator and the denominator in relation (3.14) by $\sin \theta'$ and substituting relation (3.15), f is expressed as:

$$f = \frac{\rho}{\cos \phi' - \eta \cos \theta'}. \tag{3.16}$$

Squaring both sides of relation (3.15), substituting $\sin^2 \phi' = 1 - \cos^2 \phi'$ and $\sin^2 \theta' = 1 - \cos^2 \theta'$, and solving for $\cos \phi'$, then

$$\cos \phi' = \sqrt{1 - \eta^2 + \eta^2 \cos^2 \theta'} \ . \tag{3.17}$$

For $0 < \theta' \leq \frac{\pi}{4}$, an approximation of the right-hand side of relation (3.17) gives $\cos \phi' = 1 - \eta + \eta \cos \theta'$ which, when substituted into (3.16), yields:

$$f = \frac{\rho}{1 - \eta} \ , \tag{3.18}$$

where f is the focal length measured from the center of the lens, ρ is the radius of the hemisphere, and η the relative refractive index. Thus, if only f or ρ is known, the other may be evaluated from (3.18). Even if η is not known, it may be estimated with simple experimental methods. A more reliable approximation for relation (3.17), which is valid for $0 < \theta' \leq \frac{\pi}{2}$ (the whole range of θ'), is obtained by using the binomial series. Such an approximation, however, will result in a relation that involves θ'. Relation (3.16) becomes:

$$f = \frac{2\rho}{2 - \eta^2 \sin^2 \theta' - 2\eta \cos \theta'} \ , \tag{3.19}$$

which is a complicated relation to apply.

Referring, once more, to Figure 3.3, and calling the distance from the object r' to the center of the hemisphere R, it is known that

$$\frac{1}{R} + \frac{1}{D} = \frac{1}{f} \ , \tag{3.20}$$

assuming that K is the principal point of the lens. For an object at an infinite distance from K, that is, as R approaches ∞, 1/R approaches 0. Relation (3.20) then yields to:

$$\frac{1}{D} = \frac{1}{f} \text{ or, } D = f. \tag{3.21}$$

Substituting (3.21) into (3.9), a much simpler relation, compared to (3.13), is obtained for r:

$$r = \frac{f\eta r'}{\sqrt{R^2 + (1 - \eta^2)(r')^2}}, \tag{3.22}$$

where f is measured from the center of the hemispherical lens. Relation (3.22) is generally valid since the value of R is always much greater than that of D, or f, for a camera lens system.

Any of the above derivations for r, therefore, may be employed to geometrically correct a fish-eye lens image. To determine the exact rectangular coordinates (x,y) of the pixels in the corrected image located on a plane a distance R from the lens, one may proceed as follows. Consider again the side view of the fish-eye lens as shown in Figure 3.1, page 22. A point, B', on the corrected image plane, which corresponds to the point, B, on the fish-eye image would project to B along a ray which is normal to the spherical lens at the point of intersection with the lens surface. Any line (ray) that is normal to the surface of a sphere at the point of intersection must pass through the center of the sphere. Since the center of the sphere and the focal point project as the same point, there is no bending of

the surface normal to the focal point in the (x,y) coordinate system. The ray is only diverted along the z-axis. Therefore, the angle α from a horizontal axis will be exactly the same in both the fish-eye image and the geometrically corrected image. Since the coordinates of the corrected image are known relative to the chosen center pixel of the image plane, α can be determined. Therefore, the exact pixel coordinates of the corresponding point in the fish-eye image may be found by:

$$x_0 = r \cos \alpha, \text{ and } y_0 = r \sin \alpha \tag{3.23}$$

where the coordinates (x_0,y_0) are relative to the coordinates of the center pixel of the fish-eye image.

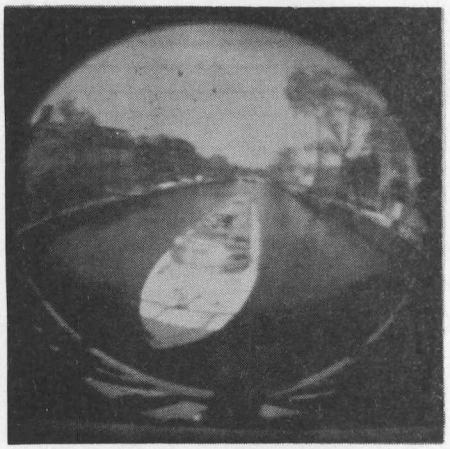
With all of the above in mind, an algorithm may be developed to geometrically correct and restore the fish-eye image. The major steps of such an algorithm are given below:

1. Obtain f (focal length) from the lens specification and calculate the relative refractive index, n, from the two known media involved.
2. Locate the center of the fish-eye image.
3. Compute r' for each pixel of the new image from (x',y').
4. Find r from relation (3.22).
5. Compute the corresponding pixel in the fish-eye image to get (x_0,y_0) using relation (3.23).

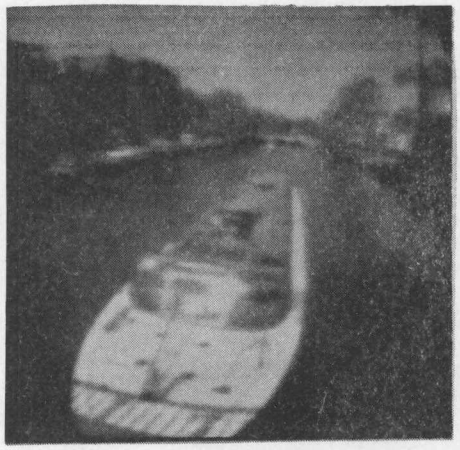
6. Place the gray level found at (x_0,y_0) at location (x',y') in the corrected image.

The above algorithm has been realized in a computer program given in Appendix A. This program was employed for correction of several fish-eye digital images. An example of the correction algorithm applied to a fish-eye camera image is shown in Figure 3.4. The original fish-eye image taken from a photograph and then digitized is shown in Figure 3.4(a). Note the curvature of the shadow of the bridge rail, as well as the large distortion in pixels near the outer radius. The image was digitized and displayed at 512 by 512 point resolution. The central 256 by 256 region of the original image, shown in Figure 3.4(b), was selected for processing. The distortion corrected image is shown in Figure 3.4(c). Note that the bridge shadow has been straightened, as well as the buildings near the outer radius, which appear to have less distortion than originally.

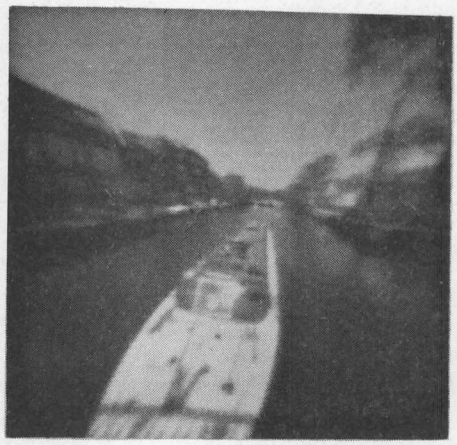
Although in the previous example the centered portion of the original image was processed, as suggested by step 2 of the correction algorithm, a portion other than the centered one may be desired for processing. It is possible to process and undistort any portion of the original image with no changes of the correction algorithm. The only difference would be in step 2 where instead of locating the center of the fish-eye image, the center of the desired area to be processed of the fish-eye image should be located.



(a)



(b)



(c)

Figure 3.4. Example of correction procedure.

(a) Original fish-eye lens image (512 x 512).
(b) Selected central section (256 x 256).
(c) Corrected central section (256 x 256).

When processing, however, only a portion of the original image, the final corrected image appears magnified. This is due to the fact that the small portion is displayed as the same size image as the original one. The result of such magnification is an increase of the blurring of the corrected image. Methods for improving the quality of a blurred picture will be discussed in Chapter V.

CHAPTER IV

RESOLUTION AND ERROR ANALYSIS

To investigate the question of resolution and restoration for the fish-eye system, the concept of a space invariant optical system is required. A brief review of this theory is necessary to determine the spread function of the present system.

The object function $O(x_o,y_o,z_o)$ may be described by

$$O(x_o,y_o,z_o) = \iiint O(x,y,z)\,\delta(x-x_o,y-y_o,z-z_o)\,dxdydz, \qquad (4.1)$$

obtained by the sifting property of the delta function. The response of a linear system, H, to this object function may be described by $I(x_1,x_2,x_3) = H[O(x_o,y_o,z_o)]$, where if (4.1) is substituted, gives:

$$H[O(x_o,y_o,z_o)] = H\left\{\iiint O(x,y,z)\,\delta(x-x_o,y-y_o,z-z_o)\,dxdydz\right\}. \qquad (4.2)$$

Since the system is assumed to be linear, relation (4.2) may be written as:

$$H[O(x_o,y_o,z_o)] = \iiint O(x,y,z)\,H\{\delta(x-x_o,y-y_o,z-z_o)\}\,dxdydz. \qquad (4.3)$$

Note that $O(x,y,z)$ is a constant with respect to the linear system computation. Therefore, the point spread function of this system is $H\{\delta(x-x_0,y-y_0,z-z_0)\}$ which may either vary with the position of the object point and image point in which case the system would be called space variant, or it may depend only on the difference in location, i.e., $H(x-x_0,y-y_0,z-z_0)$, and, thus, be space invariant [10].

To illustrate that the fish-eye lens system is a space variant one, the case in which object points on a plane, $z = k$, are imaged onto an image plane located at $z = -D$ with respect to the lens center will be considered, where k is a constant. If for such an arrangement the lens system is shown to be space variant, then it can be safely concluded that the system is space variant in general.

Consider the geometrical transformation between any object point with coordinates (x,y,z) and any image point with coordinates (x_1,x_2,x_3) as shown in Figure 4.1. Then, x and y may be expressed in spherical coordinates as:

$$x = R \sin\theta \cos\alpha, \text{ and } y = R \sin\theta \sin\alpha. \tag{4.4}$$

Also, x_1 and x_2 may be expressed as:

$$x_1 = r \cos\alpha, \text{ and } x_2 = r \sin\alpha. \tag{4.5}$$

If r is substituted from relation (3.2) into relation (4.5), x_1 and x_2 become:

$$x_1 = D \tan\phi \cos\alpha, \text{ and } x_2 = D \tan\phi \sin\alpha. \tag{4.6}$$

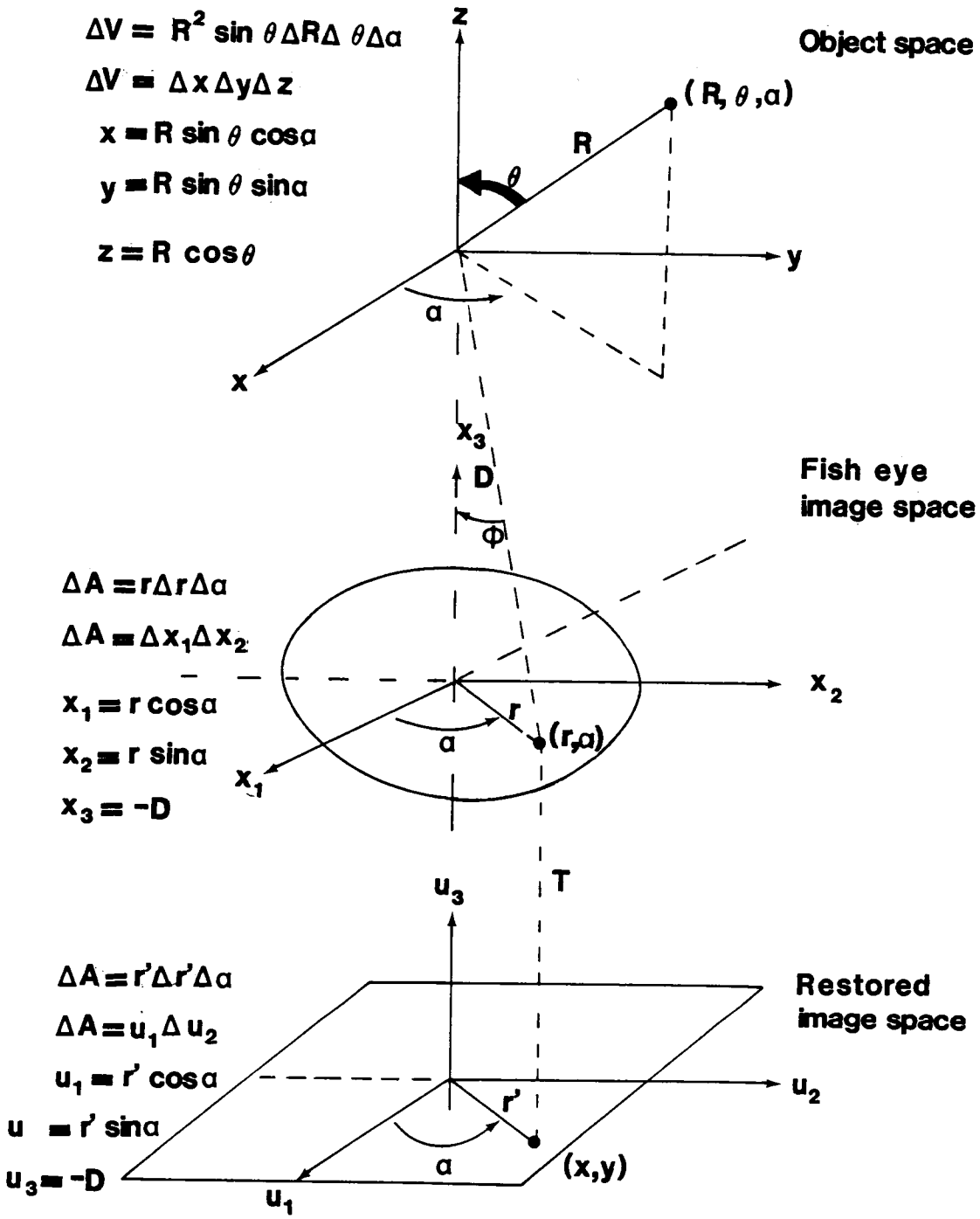


Figure 4.1. Restoration mappings and transformations.

Solving in relation (4.6) for cos α and sin α, respectively, and substituting into (4.4) then, x and y are expressed as:

$$x = \frac{R \sin \theta}{D \tan \phi} x_1, \text{ and } y = \frac{R \sin \theta}{D \tan \phi} x_2. \tag{4.7}$$

That is, relation (4.7) describes the transformation from coordinates (x,y) to coordinates (x_1,x_2). The Jacobian of the above transformation may be found to be:

$$J(x_1,x_2) = \begin{vmatrix} \frac{\partial x}{\partial x_1} & \frac{\partial x}{\partial x_2} \\ \frac{\partial y}{\partial x_1} & \frac{\partial y}{\partial x_2} \end{vmatrix} = \begin{vmatrix} \frac{R \sin \theta}{D \tan \phi} & 0 \\ 0 & \frac{R \sin \theta}{D \tan \phi} \end{vmatrix} = \frac{R^2 \sin^2 \theta}{D^2 \tan^2 \phi}, \tag{4.8}$$

since R and D are constants, and both θ and ϕ are independent of x_1 and x_2. This transformation may be viewed as a space variant linear filter with point spread function

$$H(x_1,x_2,x,y) = \frac{R^2 \sin^2 \theta}{D^2 \tan^2 \phi} \delta(x-x_1,y-y_1). \tag{4.9}$$

Another transformation, however, is necessary so that the restored image is obtained. Referring to Figure 4.1, a transformation may be defined from the fish-eye image space with coordinates (x_1,x_2,x_3) to the restored image space with coordinates (u_1,u_2,u_3). Both u_1 and u_2 are given by:

$$u_1 = r' \cos \alpha, \text{ and } u_2 = r' \sin \alpha. \tag{4.10}$$

Recalling relation (3.1) and substituting into (4.1), u_1 and u_2 become:

$$u_1 = R \tan \theta \cos \alpha, \text{ and } u_2 = R \tan \theta \sin \alpha. \tag{4.11}$$

Solving in relation (4.11) for cos α and sin α, respectively, and substituting into (4.6), x_1 and x_2 are expressed as:

$$x_1 = \frac{D \tan \phi}{R \tan \theta} u_1 \text{ and } x_2 = \frac{D \tan \phi}{R \tan \theta} u_2. \tag{4.12}$$

That is, relation (4.12) describes the transformation from coordinates (x_1,y_1) to coordinates (u_1,u_2). The Jacobian of this transformation is found to be:

$$J(u_1,u_2) = \begin{vmatrix} \frac{\partial x_1}{\partial u_1} & \frac{\partial x_1}{\partial u_2} \\ \frac{\partial x_2}{\partial u_1} & \frac{\partial x_2}{\partial u_2} \end{vmatrix} = \frac{D^2 \tan^2 \phi}{R^2 \tan^2 \theta}, \tag{4.13}$$

which also suggests a space variant transformation. Therefore, the overall transformation, which may also be found by first relating (x,y) and (u_1,u_2) and then evaluating the Jacobian for this transformation, is related to the product of the Jacobians $J(x_1,x_2)$ and $J(u_1,u_2)$ previously evaluated. That is, $J(\theta) = J(x_1,x_2) \cdot J(u_1,u_2) = \cos^2 \theta$ and the overall transformation then produces a point spread function

$$H(u_1,u_2,x,y) = \cos^2\theta \;\; \delta(x-u_1,y-u_2) \tag{4.14}$$

which represents a space variant system, since it depends on θ (varies with position) and not merely on the difference in location.

The above analysis suggests the form of an image restoration system shown in Figure 4.2 which consists of a geometric correction followed by a linear spatial filter. The point spread function or equivalent modulation transfer function may be selected to restore the degradation introduced by the finite sized lens elements or to reduce the effects of noise. It is, therefore, desirable to derive the Jacobian of the general transofrmation for the present system so that the point spread function can be determined. Considering the coordinate transformation in polar coordinates, α and r may be expressed as:

$\alpha = \alpha$, and, from relation (3.9),

$$r = \frac{D\eta r'}{\sqrt{R^2 + (1 - \eta^2)(r')^2}} \tag{4.15}$$

which is a continuous, monotonic function in terms of r'. Then the Jacobian of this transformation will be:

$$J = \begin{vmatrix} \frac{\partial\alpha}{\partial\alpha} & \frac{\partial\alpha}{\partial r'} \\ \frac{\partial r}{\partial\alpha} & \frac{\partial r}{\partial r'} \end{vmatrix} = \begin{vmatrix} 1 & 0 \\ 0 & \frac{\partial r}{\partial r'} \end{vmatrix} = \frac{\partial r}{\partial r'} \; . \tag{4.16}$$

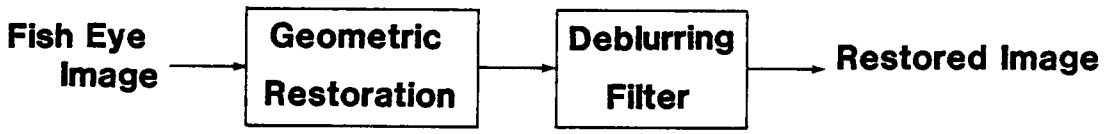


Figure 4.2. General approach to complete restoration.

Taking the first partial derivative of relation (4.15) with respect to r', the Jacobian becomes:

$$J = \frac{\partial r}{\partial r'} = \frac{D\eta R^2}{[R^2 + (1 - \eta^2)(r')^2]^{3/2}} . \tag{4.17}$$

Relation (4.17) may now be used to determine the point spread function of the fish-eye lens system, which is:

$$H(r,r') = J\ \delta(r - r'), \tag{4.18}$$

since there is no transformation for angle α.

In a similar manner, with the use of relation (3.22) in place of (4.15) or, by simply replacing D with f in (4.17), the Jacobian may be derived in terms of the focal length, f measured from the center of the hemispherical lens, and be:

$$J = \frac{f\eta R^2}{[R^2 + (1 - \eta^2)(r')^2]^{3/2}} , \tag{4.19}$$

where R is the distance of the object r' from the center of the lens and η the relative refractive index for the two media involved.

Substituting relation (4.19) into (4.18), the point spread function of the system becomes:

$$H(r,r') = \frac{f\eta R^2}{[R^2 + (1 - \eta^2)(r')^2]^{3/2}}\ \delta(r - r'). \tag{4.20}$$

Although relation (3.9) describes exactly the creation of the image r in terms of the object r', it is important to examine how

accurately a small change, Δr, of the image r, caused by a small change, $\Delta r'$, of the object r', can be determined.

Recalling relation (3.9) and letting $C = D\eta$ and $L = 1 - \eta^2$, the following relation is obtained:

$$r = G(r') = \frac{Cr'}{\sqrt{R^2 + L(r')^2}} . \tag{4.21}$$

A small change, $\Delta r'$, of r' will result in a change, Δr, of r, which is given by (exact differential)

$$\Delta r = G(r' + \Delta r') - G(r'), \tag{4.22}$$

or, substituting relation (4.21) into (4.22),

$$\Delta r = \frac{C(r' + \Delta r')}{\sqrt{R^2 + L(r' + \Delta r')^2}} - \frac{Cr'}{\sqrt{R^2 + L(r')^2}} . \tag{4.23}$$

Since r' is assumed to be small, relative to r', $(r' + \Delta r')^2 \simeq (r')^2$. Relation (4.23) now becomes:

$$\Delta r = \frac{C\Delta r'}{\sqrt{R^2 + L(r')^2}} . \tag{4.24}$$

Also, an approximation for Δr, $(\Delta r)_a$, may be determined easily with the use of the first derivative of G(r') which is an exact relation. That is,

$$(\Delta r)_a = G'(r')\, \Delta r', \tag{4.25}$$

since $\frac{\Delta r}{\Delta r'} \simeq \frac{dr}{dr'} = G'(r')$. Substituting relation (4.17) into (4.25), letting again $C = D\eta$ and $L = 1 - \eta^2$, yields:

$$(\Delta r)_a = \frac{CR^2\Delta r'}{[R^2 + L(r')^2]^{3/2}} . \tag{4.26}$$

The error, then, for the image change in terms of the object r' will be:

$$E(r') = |\Delta r - (\Delta r)_a| . \tag{4.27}$$

Substituting relations (4.24) and (4.26) into (4.27), a function for the error is obtained, after some algebraic manipulation:

$$E(r') = \frac{CL(r')^2\Delta r'}{[R^2 + L(r')^2]^{3/2}} ,$$

or, substituting back $C = D\eta$, and $L = 1 - \eta^2$,

$$E(r') = \frac{D\eta(1 - \eta^2)(r')^2\Delta r'}{[R^2 + (1 - \eta^2)(r')^2]^{3/2}} , \tag{4.28}$$

where R and D are the distances from the center of the lens to the object r' and the image r, respectively, η is the relative refractive index, and $\Delta r'$ the change of the object.

Equation (4.28) describes an error greater than the realistic one, since the relation for Δr used in (4.27) is larger than that given in (4.23). This is so, because (4.24) was obtained by replacing $(r' + \Delta r')^2$ with $(r')^2$ which is a smaller quantity; that is,

$r' + \Delta r' > r'$. However, relation (4.28) is a function of one variable, r', and all extremes may be determined. Taking the first derivative of $E(r')$ with respect to r' and setting it equal to 0, the following critical values of r' are obtained:

$$r' = 0,\ r' = \frac{\sqrt{2}\,R}{\sqrt{1-\eta^2}} \text{ and } r' = -\frac{\sqrt{2}\,R}{\sqrt{1-\eta^2}}. \tag{4.29}$$

When $r' = 0$, $E(r')$ has a minimum and it is $E_{min} = 0$. When r' equals either of the other two values in (4.29), $E(r')$ has a maximum. Since $E(r')$ is an even (symmetric) function, obtained from the symmetry of the fish-eye system, it will be sufficient if only the case for $r' > 0$ is examined. Substituting the positive value of r', from (4.29), into relation (4.28) yields:

$$E_{max} = \frac{2\sqrt{3}}{9}\,\frac{D\eta}{R}\,\Delta r', \tag{4.30}$$

where D, η and R are constant, positive quantities. For a large value of R, that is, when the object is far away from the lens, E_{max} becomes small.

In completing the examination of the error function, in terms of r', the limit of $E(r')$ as $r' \to \infty$ is evaluated and it is found to be 0. That is, as the object becomes larger and larger, the error decreases. Relation (4.28) is illustrated in Figure 4.3. This graph shows the error for $r' \geq 0$. In the case where $r' < 0$, the curve for the error is the mirror image (symmetric) of that shown in Figure 4.3. That is, as expected, the same error will be obtained with the

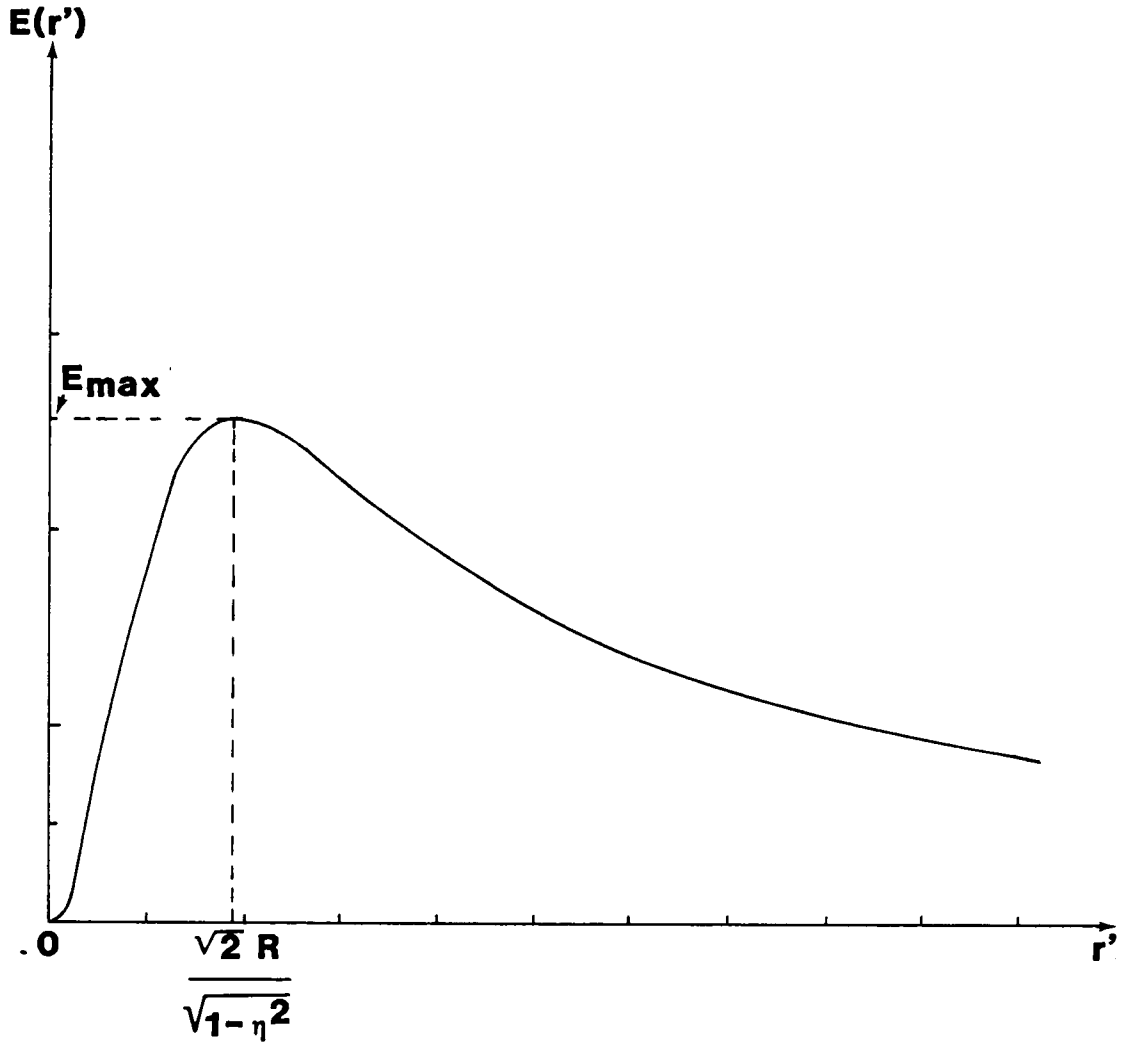


Figure 4.3. Error curve for the fish-eye lens system.

object either to the right or to the left of the central axis of the lens.

Relation (4.28) may be expressed in terms of the focal length, f, of the lens. Recalling that for large R, relative to D and f, $D \simeq f$, then (4.28) becomes:

$$E(r') = \frac{f\eta(1 - \eta^2)(r')^2\Delta r'}{[R^2 + (1 - \eta^2)(r')^2]^{3/2}}, \tag{4.31}$$

and, from relation (4.30),

$$E_{max} = \frac{2\sqrt{3}}{9}\frac{f\eta}{R}\Delta r'. \tag{4.32}$$

If the object r' is fixed and $\Delta r'$ is changing instead, then the error is given by a linear relation in terms of $\Delta r'$. From equation (4.31), or (4.28), it is apparent that the slope of this line is

$$\frac{f\eta(1 - \eta^2)(r')^2}{[R^2 + (1 - \eta^2)(r')^2]^{3/2}}, \text{ or, } \frac{D\eta(1 - \eta^2)(r')^2}{[R^2 + (1 - \eta^2)(r')^2]^{3/2}}, \tag{4.33}$$

respectively. Both quantities in (4.33) are positive. Therefore, since the slope is positive, the error increases as $\Delta r'$ increases.

It is rather interesting to examine the position of the object when the maximum error occurs. As has been shown, relation (4.30) holds true when

$$r' = \frac{\sqrt{2}\,R}{\sqrt{1 - \eta^2}}. \tag{4.34}$$

Recalling relation (3.1) and equating it with relation (4.34) yields:

$$R \tan \theta = \frac{\sqrt{2}\, R}{\sqrt{1 - \eta^2}} ,$$

or, solving for θ,

$$\theta = \tan^{-1} \sqrt{\frac{2}{1 - \eta^2}} . \qquad (4.35)$$

That is, the incident angle θ can be determined, since η is a known constant for the two media involved. Therefore, the maximum error occurs from a point located a distance R from the lens surface with an incident angle θ as given by (4.35). A different value for θ is obtained for different media involved. For the case where the two media are air ($\eta_\theta = 1$) and glass ($\eta_\phi = 1.5$) for outside the lens and the lens itself, respectively, $\eta = 0.66$ and the incident angle θ, evaluated from relation (4.35), is equal to 62.24°. The graph in Figure 4.3 was obtained with the same, as above, value of η.

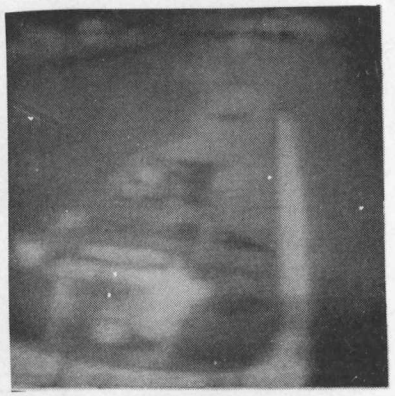
CHAPTER V

DEBLURRING OF THE RESTORED IMAGE

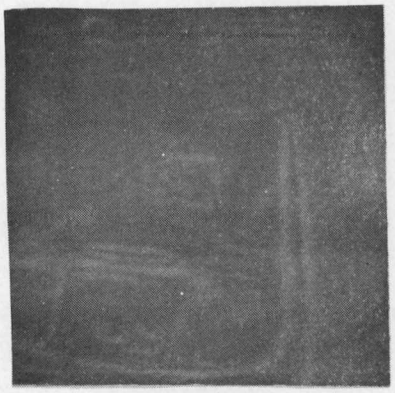
The deblurring of a picture is an interesting problem, and several approaches to its solution have been suggested since Image Processing Theory started developing. However, there are several reasons that could cause an image to be blurred; uniform motion of an object, for example, could result to a blurred image; blurring due to defocusing or magnification are also two other cases commonly encountered in processed images.

Although the basic methods for improving such blurred images consist of filtering techniques, each case of blurring requires a unique method, and perhaps filtering, for restoring such images.

As was mentioned in Chapter III, when processing a portion of the original fish-eye image, the final corrected image appears magnified. In addition, the correction algorithm (see program in Appendix A) offers a choice of an output diameter. That is, the area of the output (corrected) image may be selected and displayed as a 256 by 256 digital image. The result of this process is magnification and, thus, blurring due to magnification. In Figure 5.1(a), an output image with diameter equal to 13.33 is shown, while Figure 3.4(c), page 37, shows an image with diameter equal to 40. Both images are processed portions of the original fish-eye lens image shown in Figure 3.4(a). The magnification and the increased amount of blurring of the image in Figure 5.1(a) are apparent.



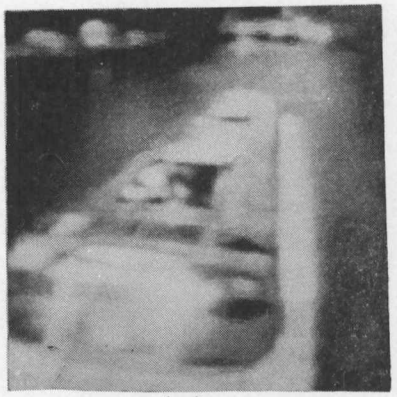
(a)



(b)



(c)



(d)

Figure 5.1. Example of the deblurring procedure.

(a) Original image.
(b) Image resulting from high-pass filtering.
(c) Image resulting from adding image in (a) to image in (b).
(d) Image resulting from equalization of image in (c).

Therefore, the blurring of an image due to magnification must be examined; a problem encountered when the analog function of optical zoom is simulated by a digital system. It is necessary to keep in mind that constant sharpness of the corrected output image must be maintained while the magnification is changing.

The consideration of the human visual system in developing a reliable technique may be necessary, since the objective is to maintain visual sharpness. As discussed in a recent article by Fahnestock and Hunt [11],

> The area under the product of the eye modulation transfer function and the modulus of the Fourier transform of the perceived-brightness-image has been shown to relate well to perceived image quality.

Also,

> Since image sharpness can change the perceived quality of an image, it is believed that a relationship exists between image sharpness and the modulus of the image Fourier transform.

On this concept the use of highpass filters is based, making images appear sharper. As the frequency increases, the Fourier transform of an image is monotonically decreasing. The image details increase and become visible when the image is magnified. This corresponds to a shifting of the modulus amplitudes found at higher frequencies to lower frequencies.

One approach, therefore, could be the application of a filter to the output magnified image that would increase the transform modulus as compared to that of the original fish-eye image. Such a filter, however, would cause a sharpening, as well as noticeable changes to the tonal characteristics of the image [11].

A second approach, which is the one adopted in this study, would be the designing of a filter which would affect only the higher frequencies of the image. Such a filter would cause almost no noticeable changes to the tonal characteristics of the image, since tonal characteristics are related to lower frequencies. In fact, an image can be blurred by eliminating high-frequency information, since edges are related to high-frequency components, and sharpened by eliminating low-frequency information without affecting high-frequency components of the Fourier transform of the image, in which case a "highpass filtering" process is employed [12].

Assuming that the Fourier transform of an image, t(x,y) to be processed, is T(v,w), where (v,w) are the coordinates of points on the frequency plane, and R(v,w) is the transform of the resulting image after the filtering process, then, R(v,w) and T(v,w) are related as follows:

$$R(v,w) = F(v,w)\ T(v,w) \tag{5.1}$$

where F(v,w) is the transfer function of the filter used. Therefore, if the inverse Fourier transform of R(v,w) is taken, then, the desired restored (corrected) image r(x,y) will be obtained, since the undesired frequencies have been "filtered out" due to the presence of F(v,w) in relation (5.1).

There are four types of highpass, and lowpass, filters that are commonly well known and used: the Ideal Filter, the Butterworth Filter, the Trapezoidal Filter, and the Exponential Filter [12].

Each of these filters will be discussed briefly before the analytical steps of the technique used are described.

Ideal Highpass Filter

The transfer function, F(v,w), of the ideal highpass filter is given by the relation

$$F(v,w) = \begin{cases} 0 \text{ if } d(v,w) \leq \varepsilon_0 \\ 1 \text{ if } d(v,w) > \varepsilon_0 \end{cases} \tag{5.2}$$

where ε_0 is a cut-off distance measured from the origin of the frequency plane, and $d(v,w) = \sqrt{v^2 + w^2}$, that is, the distance from point (v,w) to the origin of the frequency plane. This filter will eliminate all frequencies inside a circle of radius ε_0 while not affecting frequencies outside the circle. Unfortunately, however, the ideal filter cannot be realized physically [12].

Butterworth Highpass Filter

The transfer function, F(v,w), of the Butterworth highpass filter is given by the relation

$$F(v,w) = \frac{1}{1 + [\varepsilon_0/d(v,w)]^{2k}} \tag{5.3}$$

where ε_0 and d(v,w) have been specified above, and k is the order of the filter. When $d(v,w) = \varepsilon_0$, then, F(v,w) is equal to 1/2 of its maximum value. It is common, however, that in the case of the Butterworth filter ε_0 is selected so that F(v,w) is equal to $1/\sqrt{2}$ its

maximum value [12]. In that case, relation (5.3) is rearranged as follows:

$$F(v,w) = \frac{1}{1 + 0.414[\varepsilon_0/d(v,w)]^{2k}} \tag{5.4}$$

where all variables have been specified above.

Trapezoidal Highpass Filter

The transfer function, F(v,w), of the trapezoidal highpass filter is given by the relation

$$F(v,w) = \begin{cases} 0 & \text{if } d(v,w) < \varepsilon_1 \\ \dfrac{d(v,w) - \varepsilon_1}{\varepsilon_0 - \varepsilon_1} & \text{if } \varepsilon_1 \leq d(v,w) \leq \varepsilon_0 \\ 1 & \text{if } d(v,w) > \varepsilon_0 \end{cases} \tag{5.5}$$

where d(v,w) and ε_0 have been specified earlier, and ε_1 is arbitrary as long as it is less than ε_0 [12].

Exponential Highpass Filter

The transfer function, F(v,w), of the exponential highpass filter is given by the relation

$$F(v,w) = \exp\{-[\varepsilon_0/d(v,w)]^k\} \tag{5.6}$$

where d(v,w) and ε_0 have been specified earlier, and k is a parameter on which the rate of increase of F(v,w) depends. When $d(v,w) = \varepsilon_0$, then, F(v,w) = 1/e. Again, as in the Butterworth highpass filter, it

is common that ε_0 is selected so that F(v,w) is equal to $1/\sqrt{2}$ of its maximum value [12]. In this case, relation (5.6) is rearranged as follows:

$$F(v,w) = \exp\{-0.347[\varepsilon_0/d(v,w)]^k\} \tag{5.7}$$

where all variables have been specified above.

In attempting to develop a process which will result in an improved image, recall that sharpening of the edges will emphasize the information within their boundaries and, thus, eliminate some blurring. The Exponential Highpass Filter will be employed in the process described below.

Consider the block diagram of Figure 5.2. Assume that an image, t(x,y) originally blurred is to be processed and it is desired that the highpass exponential filter is applied. Before doing so, however, it is necessary, as suggested by relation (5.1), that the image is presented in the frequency domain; that is, transform the image, t(x,y), from its real domain to its complex one and obtain T(v,w). This can be achieved by using the forward two-dimensional Fast Fourier Transform (FFT) given in Appendix B. Now that the image is presented in the frequency domain, the highpass exponential filter given by relation (5.6) can be applied. In this case, k = 2, where the filter is referred to as a "second order highpass exponential filter," and ε_0 = 128 were chosen. Since a highpass filter has been applied, the low frequencies of the image were eliminated, while the high frequencies, which represent the edges, remained. The resulting

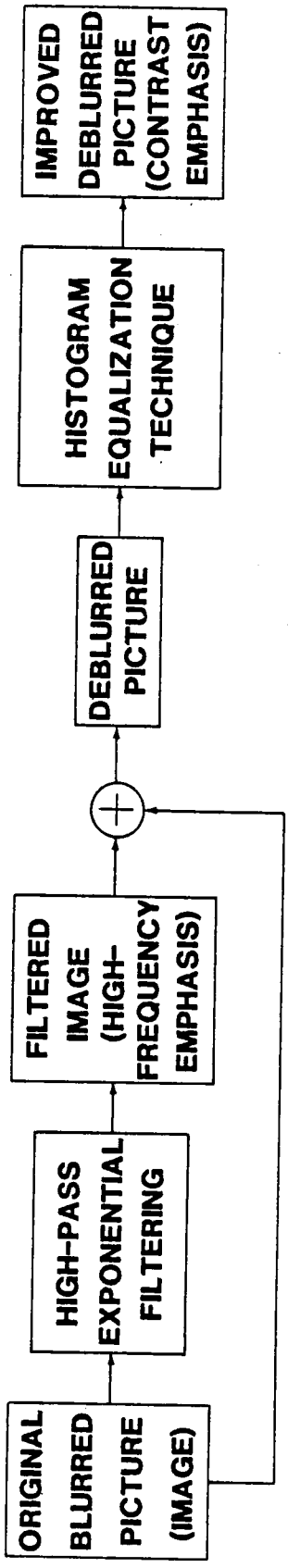


Figure 5.2. Detailed procedure for improving a blurred image.

image, however, R(v,w), is still presented in the frequency domain. To obtain the image in the real domain, r(x,y), the inverse FFT must be applied. The process, up to this point, of the blurred image in Figure 5.1(a), page 54, will result in the image in Figure 5.1(b), where only the edge of elements have been maintained.

As a next step to this procedure, the filtered image shown in Figure 5.1(b) is added to the original one so that all information necessary for a complete image is obtained simultaneously with the emphasis of the edges, which will result in a partially deblurred image. The outcome of this addition, which is performed pixel by pixel, is shown in Figure 5.1(c).

As a last step to this deblurring process, a technique known as the histogram equalization technique [1] is applied to the image of Figure 5.1(c). Such a technique will increase the contrast of the image and, since the picture has been partially deblurred, a greater amount of detail will be revealed. The image resulting from histogram equalization is shown in Figure 5.1(d).

In general, by "histogram equalization" is meant an arrangement or distribution of the gray levels of an image so that their density is uniform [1], thus increasing the dynamic range of the pixels of the image. It will be shown that there is a transformation of the gray levels of an image to levels with uniform density.

Assume that g describes the gray levels of the pixels of an image. If the value 0 refers to black and value 1 to white in the gray level scale, then $0 \leq g \leq 1$. Since the gray levels of an image

are random values, assuming that g is a continuous variable, they can be described by their probability density function $\Pi(g)$. Then, the new gray levels g_ν corresponding to every pixel value g of the original image may be defined as [12]

$$g_\nu = \int_0^g \Pi(\lambda)d\lambda;\ 0 \leq g \leq 1; \tag{5.8}$$

where λ is a dummy variable for the integration.

Relation (5.8), however, would be applicable to digital image processing if it were given in a discrete form, since the pixels of an image are finite in number and are not described by a continuous function. Calling N the number of gray levels, σ the number of pixels of an image, and n_i the number of times the ith gray level appears in an image, then the discrete probability $\Pi(g_i)$ is [1]

$$\Pi(g_i) = \frac{n_i}{\sigma}\ , \tag{5.9}$$

with $0 \leq g_i \leq 1$ and $i = 1,2, \ldots , N$. Therefore, the discrete form of relation (5.8) may be obtained relating the new gray levels $(g_\nu)_i$ corresponding to every pixel value g_i of the original image. This discrete form, expressed as a sum, is given below [1]:

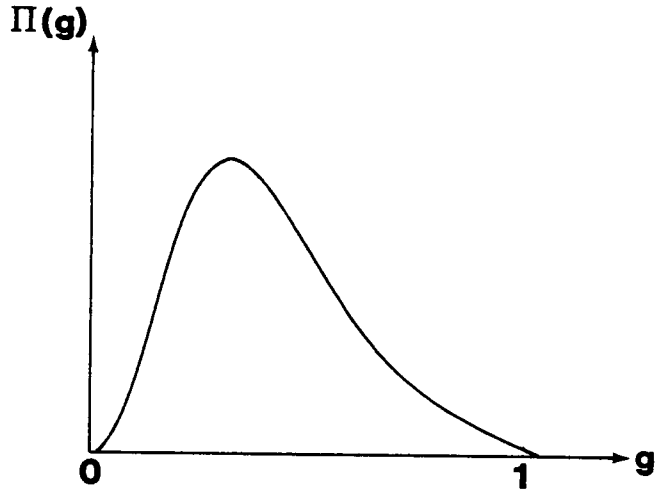
$$(g_\nu)_i = \sum_{j=1}^{i} \Pi(g_j) = \sum_{j=1}^{i} \frac{n_j}{\sigma} \tag{5.10}$$

with $0 \leq g_i \leq 1$ and $i = 1,2, \ldots , N$; where N is the number of levels.

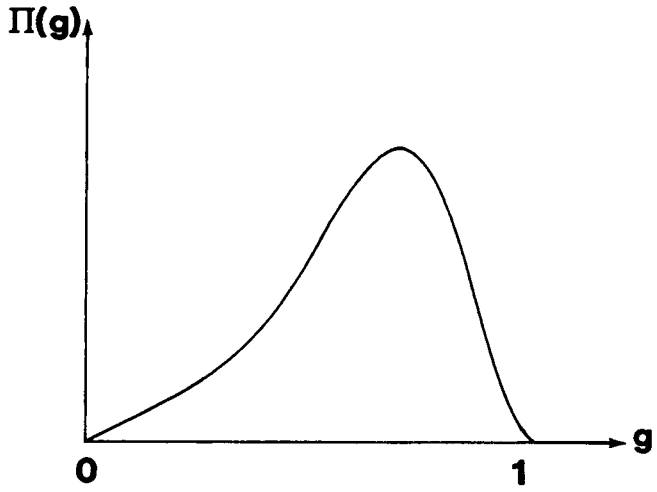
In general, the density function of the gray levels of an image is a source of information about the characteristics of that image. Figure 5.3(a) shows the density function of an image with dark characteristics, while Figure 5.3(b) represents an image with light characteristics.

The histogram (gray level density function) of the image in Figure 5.1(c), page 54, is shown in Figure 5.4(a), and the histogram of the equalized image in Figure 5.1(d) is shown in Figure 5.4(b). It is apparent that the histogram equalized image in Figure 5.1(d) is a much sharper image, revealing clearer details, compared to the images of Figures 5.1(a) and 5.1(c).

With the geometric restoration and the deblurring process applied, a complete correction of an image has been developed.



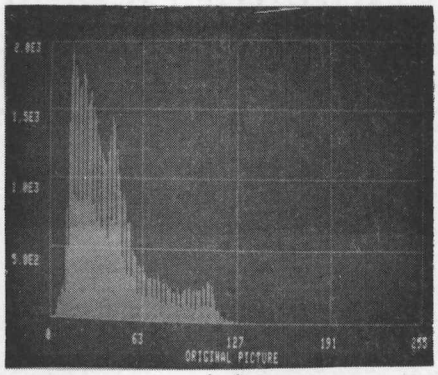
(a)



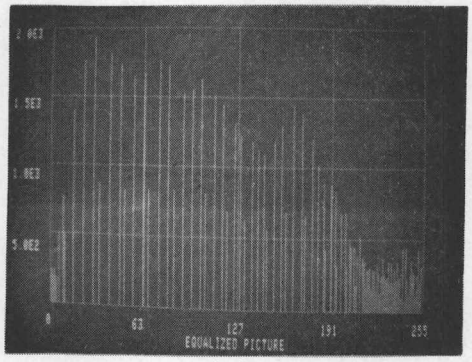
(b)

Figure 5.3. Illustrations of density functions.

(a) Represents a "dark" image.
(b) Represents a "light" image.



(a)



(b)

Figure 5.4. Histograms of images.

(a) Histogram of image in Figure 5.1(c).
(b) Histogram of image in Figure 5.1(d); equalized.

CHAPTER VI

CORRECTION SYSTEM DESCRIPTION

Since the methods for correcting a fish-eye image have been determined, it is desirable that a general description of an applicable system is presented, including both the recognition and the analysis of digitized pictures.

An image correction system is shown in Figure 6.1 in the form of a block diagram. This system consists of an arrangement of two 220° field of view, fish-eye lenses that would provide full 4π steradian coverage, as well as redundant information along the overlapping radial picture elements. Through the camera system, a given region of interest could be selected for correction and display. This "foveal" [13] viewing arrangement would operate in a manner similar to the high resolution foveal area in the human eye which permits an area of interest in a scene to be mapped onto a small high resolution array of detectors. The major difference, however, between the human eye's mechanism and the proposed one is that the lens would remain fixed, only the detector array would move, as opposed to other imaging systems that must move a bulky camera and lens system. Only linear translation of the high resolution array in the image plane would be required to cover the entire fish-eye image.

When the image is received from each camera, it would then be digitized and stored in the frame buffers, as shown in Figure 6.1. Two buffers are necessary to accommodate overlapping selected

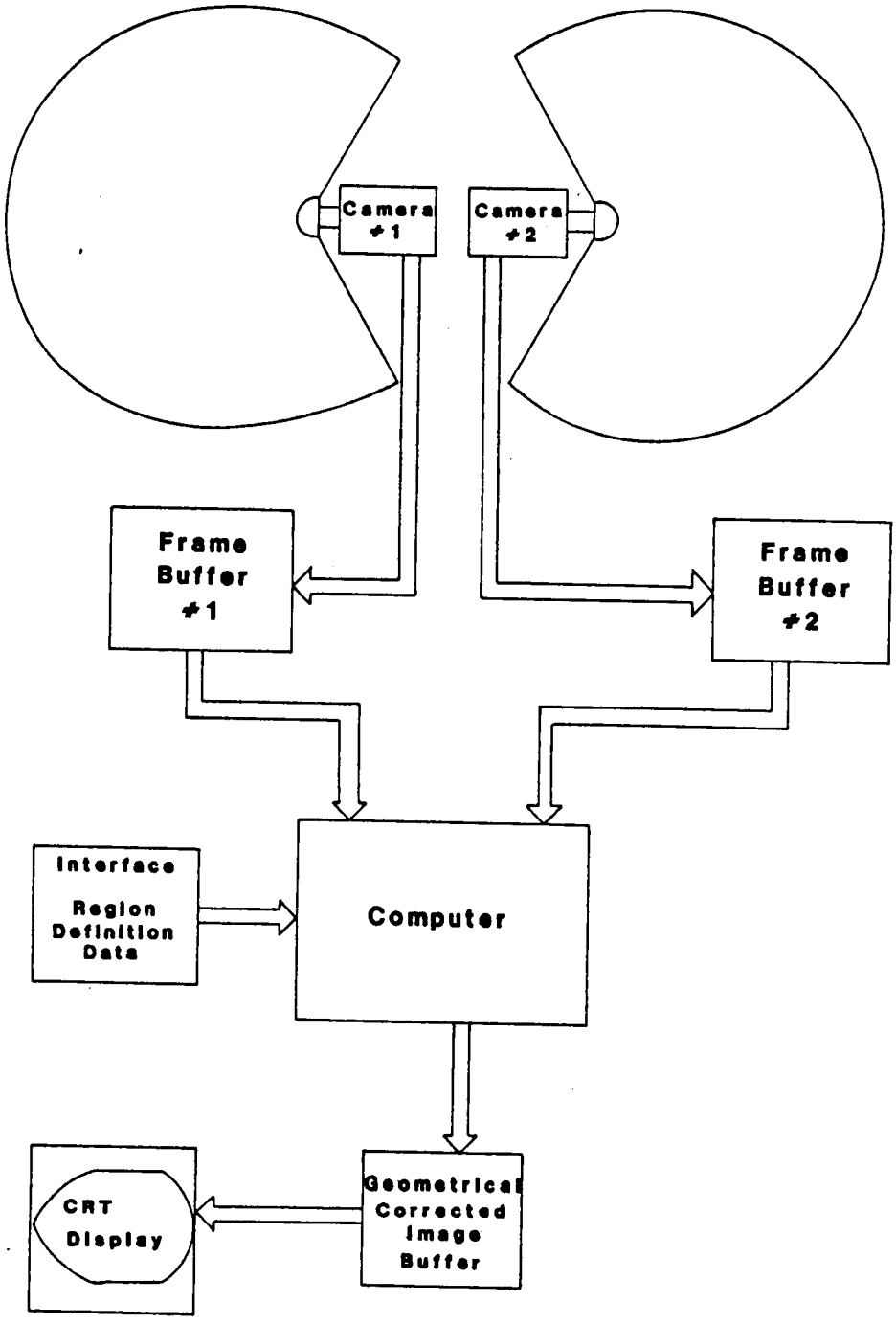
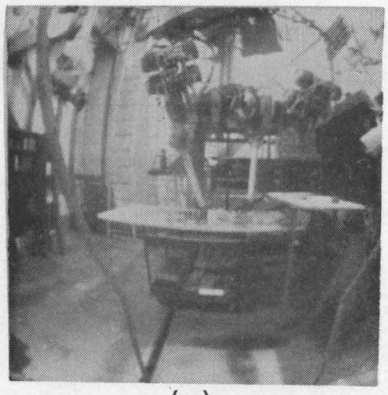


Figure 6.1. Block diagram of correction system.

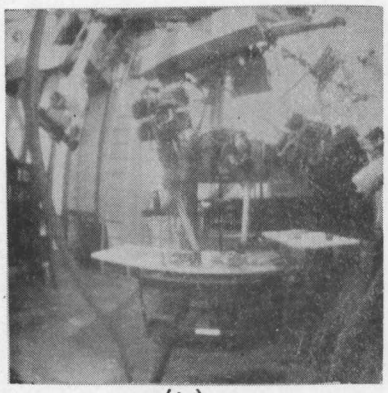
regions. A computer would control the operator interface for region selection and via table look-up would also complete the image corrections employing the correction algorithm proposed in Chapter III. The geometrically corrected image would be further processed for sharpening, if desired, and then finally displayed on the CRT, as shown in Figure 6.1.

The proposed system is applicable not only to static images, but also to a sequence of images that describe, for example, motion. This can be developed by simply correcting individually each scene of the sequence. Although such a process appears to be extremely time consuming, it requires less time than processing the scenes as if they did not belong in a sequence. In fact, when a motion sequence, with an object always moving within the area of the lens field, is to be processed, the following method may be employed. The first image is processed and corrected normally as a whole. The second and following images are not processed as the first; instead, each is subtracted from the previous one and only the difference of the two is corrected, since motion is made noticeable because of position differences. The above method is based on the concept of human vision which is made possible because of differences in scenes. The time required to subtract two 512 by 512 fish-eye lens images is less than that required to correct and restore one fish-eye lens image.

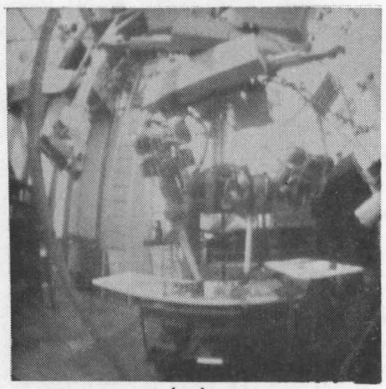
Figure 6.2 shows four original fish-eye lens images that describe a sequence of a vertical camera motion. Figure 6.3 also contains four images that describe vertical motion; however, they are



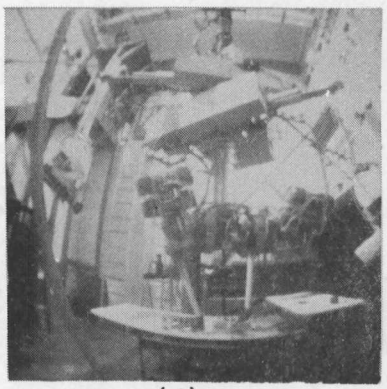
(a)



(b)

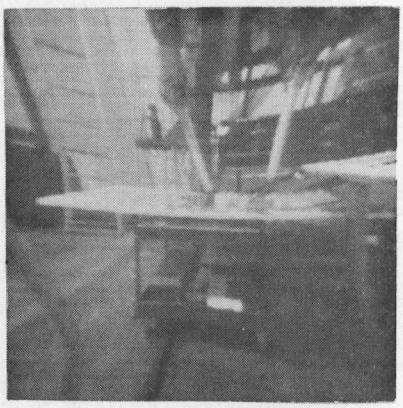


(c)

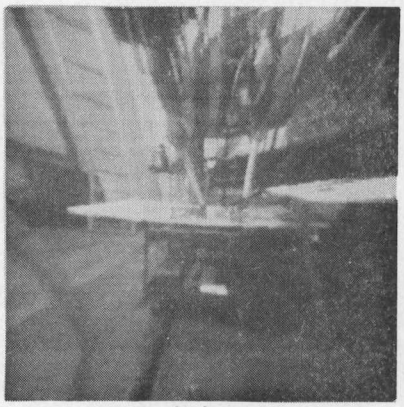


(d)

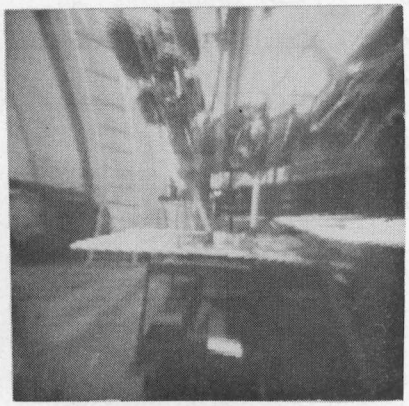
Figure 6.2. Four fish-eye images describing a vertical motion sequence.



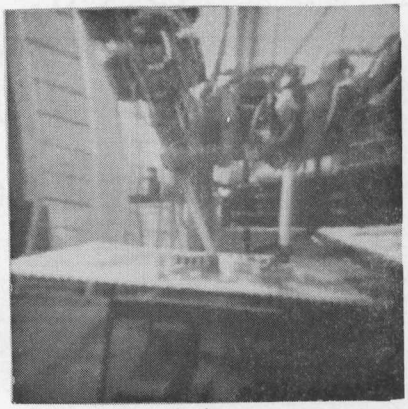
(a)



(b)



(c)



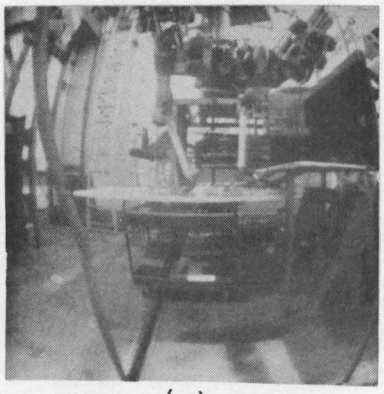
(d)

Figure 6.3. Partially corrected images corresponding to those in Figure 6.2.

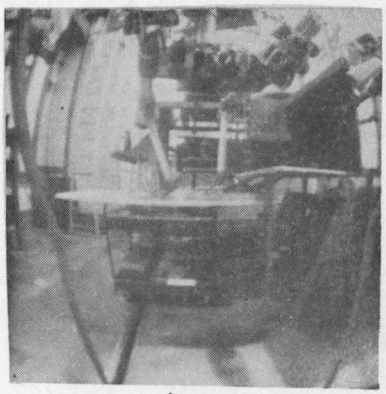
partially corrected portions of the images in Figure 6.2. In addition, Figure 6.4 contains four fish-eye images that describe horizontal motion. The corresponding geometrically corrected portions of the images in Figure 6.4 are shown in Figure 6.5. No deblurring has been applied to any of the images in Figures 6.3 and 6.5. Finally, Figure 6.6(a) shows an image taken with a 50 mm lens, while Figure 6.6(b) shows an image taken with a fish-eye lens. The image of Figure 6.6(a), although taken from a different angle, is to be used for comparison with the corrected images of the previous two sequences.

The computer system employed to accomplish the geometric and blurring corrections of the fish-eye images throughout this study was a PDP-11. The horizontal and vertical sequence images were originally recorded on a magnetic tape. With the use of a computer program, given in Appendix C, these images were transferred to magnetic disks, with which the PDP-11 system operates, and then processed with the previously suggested methods.

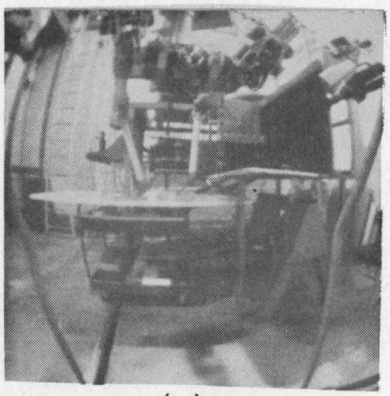
It is interesting to note that the curvature of the table shown on the images in Figures 6.2 and 6.4 has been straightened on the corrected images in Figures 6.3 and 6.5, respectively. Although, as was mentioned earlier, the image in Figure 6.6(a) is to be compared with the corrected ones, it is important to keep in mind that this image was digitized and displayed at 512 by 512 point resolution, while the images in Figures 6.3 and 6.5, in addition to their magnification, were displayed at a 256 by 256 point resolution.



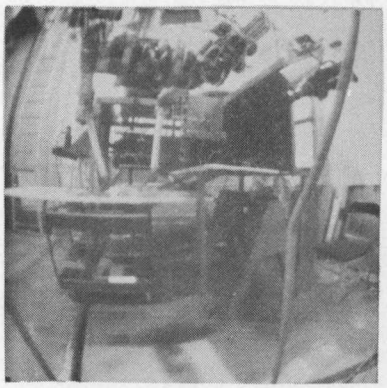
(a)



(b)

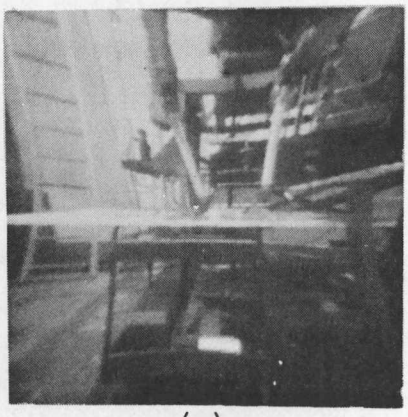


(c)

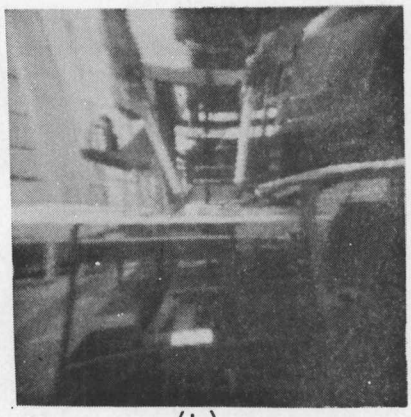


(d)

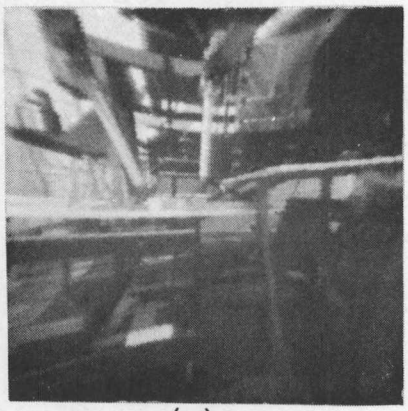
Figure 6.4 Four fish-eye images describing a horizontal motion sequence.



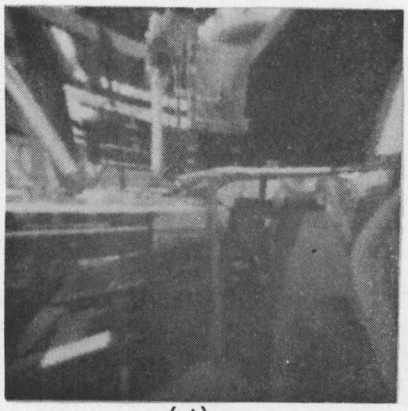
(a)



(b)

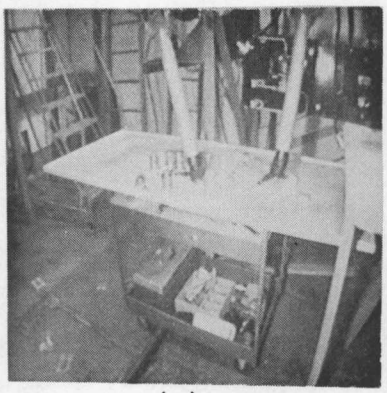


(c)

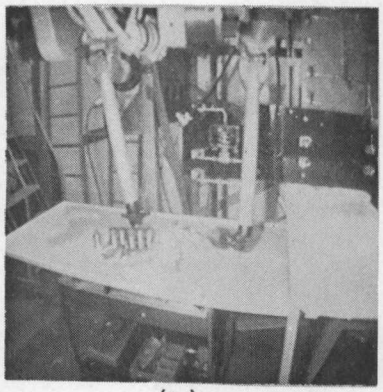


(d)

Figure 6.5 Partially corrected images corresponding to those in Figure 6.4.



(a)



(b)

Figure 6.6 A normal 50 mm lens image and a fish-eye lens image.

(a) Taken with a 50 mm lens.
(b) Taken with a fish-eye lens.

CHAPTER VII

CONCLUSIONS

This study of methods for omnidirectional imaging has illustrated the procedures which may be employed for restoration of both geometric distortion and blurring.

This type of imaging appears useful for many applications. For example, an omnidirectional vision system could permit a robot to detect objects in all directions and enable it to select optimum paths for obstacle avoidance. In addition, a mobile robot would require no power for mechanical scanning, since it would be able to cover a 2π, or 4π if two lenses are used, steradian field of view. In security applications, the "blind area" of the existing camera systems would be eliminated. In stereoscopic object location applications, the azimuthal range for which an object is simultaneously visible in both stereo views would be greatly extended. Also, omnidirectional viewing could eliminate multiple x-ray images necessary for detecting the stomach or other parts of the body.

The simplicity of recording an entire scene with a single image is considered a definite advantage, even with the computations required in the restoration process. With the steadily increasing power of microcomputers, coupled with steadily decreasing hardware costs, it does not appear that it is overly optimistic to assume that the processing power necessary for real time implementation will be available at a modest cost in only four to five years.

Further analysis, however, is required to understand spectral, temporal, and noise effects, as well as to consider applications such as target tracking, stereoscopic viewing, exact image recognition, and even processing color fish-eye lens images. In addition, methods must be developed for recognizing and correcting causes that result in blurred images. The filtering procedures developed up to date do not generally apply to all types of blurring. The "Homomorphic" [12] filtering process, for example, is applicable only to images with loss of sharpness, while the "Weiner" [1] filter is applicable to blurred images which also contain noise. Therefore, a detailed investigation of all aspects of a fish-eye lens image is necessary before the appropriate correction methods are employed.

LIST OF REFERENCES

LIST OF REFERENCES

[1] E. L. Hall, Computer Image Processing and Recognition, Academic Press, 1979.

[2] J. M. Franke, "Field Widened Pinhole Camera," Applied Optics, Vol. 18, No. 17, pp. 2914, Sept. 1979.

[3] "Lens Work, The Canon Guide to Interchangeable Lenses and Single Lens Reflex Photography," Canon, Inc., Tokyo, Japan, 1981.

[4] M. Laikin, "Wide Angle Lens Systems," SPIE Volume 237, May 1980, pp. 530-534.

[5] Proceedings of the 1980 International Lens Design Conference, SPIE, Volume 237, May 1980, Oakland, CA.

[6] K. Miyamoto, "Fish Eye Lens," Journal Letter, Vol. 54, pp. 1060-1061, 1964.

[7] C. Beck, "Apparatus to Photograph the Whole Sky," Journal of Scientific Instrumentation, Vol. 2, pp. 135-139, 1925.

[8] J. C. Maxwell, The Scientific Papers, New York, 1952, pp. 78-79.

[9] Yu. N. Demkov and V. N. Ostrovskii, "Internal Symmetry of the Maxwell Fish-eye Problem and the Fock Group for the Hydrogen Atom," Soviet Physics--JETP 13, No. 6, pp. 1083-1087, December 1971.

[10] A. A. Sawchuk, "Space Variant Image Motion Degradation and Restoration," Standord University Report, SU-SEL-72-020, May 1972.

[11] J. D. Fahnestock and B. R. Hunt, "The Maintenance of Sharpness in Magnified Digital Images," Unpublished, Univ. of Arizona, Tuscon.

[12] R. C. Gonzalez and P. Wintz, Digital Image Processing, Addison-Wesley Co., Reading, Mass., 1977, pp. 118-166.

[13] R. L. Anderson, N. Alvertos, and E. L. Hall, "Omnidirectional Real Time Imaging Using Digital Restoration," Proceedings of the International Congress on High Speed Photography and Photonics, San Diego, CA, pp. 807-816, Aug. 1982.

APPENDICES

APPENDIX A

GEOMETRIC CORRECTION COMPUTER ALGORITHM

The following program corrects the geometric distortion of a wide-angle (i.e., fish-eye) lens image. Most of the program has been created by C. A. McPherson, recently graduated from The University of Tennessee, with a Master's degree in Electrical Engineering.

```
      EXTERNAL ICBCRG, ICSR, IMAGE
      COMMON /BLK1/ JCSR, JCBCRG
      COMMON /BLK2/ PIC
      COMMON /BLK3/ ICHSIZ
      LOGICAL*1 PIC(512,16), PIC1(256,32), PIX1(2)
      INTEGER*2 JCBCRG, JCSR, PIX
      EQUIVALENCE (PIX,PIX1), (PIC,PIC1)
      JCSR = IADDR(ICSR)
      JCBCRG = IADDR(ICBCRG)
      ICHSIZ = 3
      CALL IP5INI
      CALL SETUP
      CALL ZEROMS(31)
      DO 2 I = 1,1999
         I1=I
         CALL WRANNO (I1,0,1,0)
    2 CONTINUE
      CALL IPOKE(JCSR, '61000)
C
C     READ IN THE WIDE-ANGLE LENS IMAGE
C
      CALL OPNPC1(1,0,520,LOC1)
      CALL IPOKE(JCBCRG, '100000)
      CALL IPOKE(JCBCRG+2, '4777)
      CALL IPOKE(JCBCRG+4, -1)
      CALL IPOKE(JCBCRG+6, 255)
      CALL SCRLZM(1,0,0,0)
      CALL SCRLZM(2,0,0,1)
      NBLK = 9
      DO 10 I = 1,32
         ISTAT = IBRD(1,PIC,NBLK,4096,NBLK)
         CALL BLKMOV(PIC,IMAGE,4096)
   10 CONTINUE
      CLOSE(UNIT=1)
C
C     NOW DO THE TRANSFORMATION
C
      WRITE(7,200)
  200 FORMAT('$Enter the coordinates of the image center: ')
      READ(5,211) CX,CY
  211 FORMAT(2F8.3)
  210 FORMAT(2I3)
      WRITE(7,220)
  220 FORMAT('$Enter the focal length: ')
      READ(5,230) FL
  230 FORMAT(F8.3)
      WRITE(7,240)
  240 FORMAT('$Enter the lens diameter: ')
      READ(5,230) DIAM
      WRITE(7,250)
```

```
 250   FORMAT('$Enter the range of the X ordinate: ')
       READ(5,210) IXL,IXH
       WRITE(7,260)
 260   FORMAT('$Enter the range of the Y ordinate: ')
       READ(5,210) IYL,IYH
       WRITE(7,270)
 270   FORMAT('$Enter the diameter of the output image: ')
       READ(5,230) OUTD
       WRITE(7,280)
 280   FORMAT('$Enter the relative refractive index of the lens: ')
       READ(5,230) RRI
       RADIUS = DIAM/2.0
       WX = FLOAT(IXH-IXL)
       WY = FLOAT(IYH-IYL)
       DX = DIAM/WX
       DY = DIAM/WY
       ODX = OUTD/256.0
       ODY = ODX
       CALL IPOKE(JCSR, '20000)
       CALL IPOKE(JCBCRG+6,'177)
       CALL DCHAN(1)
       DO 40 M = 0,7
       DO 35 K = 0,31
          J = M*32 + K
          DO 30 I = 0,255
             DP1 = SQRT((FLOAT(I)-127.5)**2 + (FLOAT(J)-127.5)**2)
             DP = ODX * DP1
               TOP=FL*RRI*DP
             BOTOM=SQRT((RADIUS**2.0)+(1.0-RRI**2.0)*(DP**2.0))
            D=TOP/BOTOM
             GAMMA = ABS(ATAN((FLOAT(J)-127.5)/(FLOAT(I)-127.5)))
             IF(I.GE.128) X = CX + D*COS(GAMMA)/DX
             IF(I.LT.128) X = CX - D*COS(GAMMA)/DX
             IF(J.GE.128) Y = CY + D*SIN(GAMMA)/DY
             IF(J.LT.128) Y = CY - D*SIN(GAMMA)/DY
             IX = IFIX (X + 0.5)
             IY = IFIX (Y + 0.5)
             PIX = IPIX(IY,IX,JCBCRG,IMAGE)
             PIC1(I+1,K+1) = PIX1(1)
 30       CONTINUE
 35    CONTINUE
       CALL IPOKE(JCSR, '61000)
       CALL IPOKE(JCBCRG, '100000)
       IOUTY = (511 - M*32) + '4000
       CALL IPOKE(JCBCRG+2, IOUTY)
       CALL IPOKE(JCBCRG+6, '22177)
       CALL BLKMOV(PIC,IMAGE,4096)
       CALL IPOKE(JCSR, '20000)
       CALL IPOKE(JCBCRG+6, '177)
 40    CONTINUE
       CALL SAVPIC(1)
       CALL DCHAN(5)
       STOP
       END
```

All of the input variables in the above program are real numbers except the range of the x and y coordinates as shown in lines 250 and 260, respectively. In line 270, the choice of the output diameter OUTD allows a magnification of the portion of the image processed.

APPENDIX B

FAST FOURIER TRANSFORM SUBROUTINE

The following subroutine will take the Fourier transform of an image. That is, a transformation from the real domain to the complex one will occur. The inverse transform, from the complex to the real domain, can be obtained with the use of the same subroutine. It has been adapted from the book Digital Image Processing by R. C. Gonzalez and P. Wintz [1977, p. 87].

```
      SUBROUTINE FFT(F,LN)
      COMPLEX F(1024),U,W,T,CMPLX
      PI=3.141593
      N=2**LN
      NV2=N/2
      NM1=N-1
      J=1
      DO 3 I=1,NM1
      IF(I.GE.J) GO TO 1
      T=F(J)
      F(J)=F(I)
      F(I)=T
1     K=NV2
2     IF(K.GE.J) GO TO 3
      J=J-K
      K=K/2
      GO TO 2
3     J=J+K
      DO 5 L=1,LN
      LE=2**L
      LE1=LE/2
      U=(1.0,0.0)
      W=CMPLX(COS(PI/LE1),-SIN(PI/LE1))
      DO 5 J=1,LE1
      DO 4 I=J,N,LE
      IP=I+LE1
      T=F(IP)*U
      F(IP)=F(I)-T
4     F(I)=F(I)+T
5     U=U*W
      DO 6 I=1,N
6     F(I)=F(I)/FLOAT(N)
      RETURN
      END
```

The variable N is equal to the number of pixels of the image, while LN is equal to lnN/ln2, that is, the power of 2 so that 2 to the LN equals N. Variable F is the array whose transform is to be taken. Since F is complex, when the input is real, then, the imaginary part should be set equal to zero.

APPENDIX C

TAPE TO DISK TRANSFER PROGRAM

With the following computer program, the transfer of image files from an unlabeled magnetic tape to a magnetic disk is made possible. This program was created by E. L. Hall, D. D. Thompson, and N. Alvertos at the Image Processing Laboratory at The University of Tennessee, Knoxville.

```
C       DIMENSION ARRAYS
        LOGICAL*1 BUF(512),FNAME(36)
C
        CALL TAPIO(1,IERR)
        CALL REWIND
C       OPEN OUTPUT FILE
C       FIRST GET NAME
        CALL GETFNM('INPUT FILE NAME','PIC',FNAME,NCHAR)
C       NOW OPEN FILE
        OPEN(UNIT=2,TYPE='NEW',NAME=FNAME,ACCESS='DIRECT',
     1   FORM='UNFORMATTED',RECORDSIZE=128)
        CALL NEWHDR(BUF,,'L',9,512)
        WRITE(2'1)BUF
C       REQUEST NUMBER OF FILE
   10   FORMAT(I5)
        WRITE(5,20)
   20   FORMAT('$FILE NUMBER: ')
        READ(5,10)NF
        IF (NF.EQ.0) GO TO 25
        CALL SPAFIL(NF)
        IF (IERR.NE.1) GO TO 40
25      CONTINUE
        DO 30 JPP=9,520
        LBUF = 512
        CALL GETDAT(BUF,LBUF)
        WRITE(2'JPP)BUF
   30   CONTINUE
        GO TO 60
   40   WRITE(5,50) IERR
   50   FORMAT('TAPE ERROR',I5)
   60   CALL EXITAP
        STOP
        END
```

Line 20 is asking for the number of the file to be transferred from the tape to the disk. With "INPUT FILE NAME" is meant the name that the user wishes to give to the file to be transferred.

VITA

Nicolas Alvertos was born in Volos, Greece on July 22, 1957. He attended elementary school in Athens and was graduated from the High School of Paleo Faliro in June 1975. In the spring of 1976, he entered The University of Tennessee, Knoxville, and in August 1981, he received a Bachelor of Science degree in Electrical Engineering. In the fall of 1981, he was accepted at The University of Tennessee, Knoxville, where he began study toward a Master's degree. In the spring of 1982, he accepted a teaching assistantship in the Department of Nuclear Engineering and later, in the fall of 1982, in the Department of Mathematics at the same university. His Master's degree was awarded in August 1983.

Mr. Alvertos will continue his education in Electrical Engineering and begin study toward a Ph.D. degree after graduation.